

# Towards Effective and Robust Neural Trojan Defenses via Input Filtering

Kien Do<sup>1\*</sup>, Haripriya Harikumar<sup>1</sup>, Hung Le<sup>1</sup>, Dung Nguyen<sup>1</sup>, Truyen Tran<sup>1</sup>,  
Santu Rana<sup>1</sup>, Dang Nguyen<sup>1</sup>, Willy Susilo<sup>2</sup>, Svetha Venkatesh<sup>1</sup>

<sup>1</sup> Applied Artificial Intelligence Institute (A2I2), Deakin University, Australia

<sup>2</sup> University of Wollongong, Australia

<sup>1</sup> {k.do, h.harikumar, thai.le, dung.nguyen, truyen.tran,  
santu.rana, d.nguyen, svetha.venkatesh}@deakin.edu.au

<sup>2</sup> wsusilo@uow.edu.au

## Abstract

*Trojan attacks on deep neural networks are both dangerous and surreptitious. Over the past few years, Trojan attacks have advanced from using only a simple trigger and targeting only one class to using many sophisticated triggers and targeting multiple classes. However, Trojan defenses have not caught up with this development. Most defense methods still make out-of-date assumptions about Trojan triggers and target classes, thus, can be easily circumvented by modern Trojan attacks. In this paper, we advocate general defenses that are effective and robust against various Trojan attacks and propose two novel “filtering” defenses with these characteristics called Variational Input Filtering (VIF) and Adversarial Input Filtering (AIF). VIF and AIF leverage variational inference and adversarial training respectively to purify all potential Trojan triggers in the input at run time without making any assumption about their numbers and forms. We further extend “filtering” to “filtering-then-contrasting” - a new defense mechanism that helps avoid the drop in classification accuracy on clean data caused by filtering. Extensive experimental results show that our proposed defenses significantly outperform 4 well-known defenses in mitigating 5 different Trojan attacks including the two state-of-the-art which defeat many strong defenses.*

## 1. Introduction

Deep neural networks (DNNs) have achieved superhuman performance in recent years and have been increasingly employed to make decisions on our behalf in various critical applications in computer vision including object detection [35], face recognition [33, 38], medical imaging [28, 50], autonomous driving, surveillance [42] and so on. However,

many recent works have shown that besides the powerful modeling capability, DNNs are highly vulnerable to adversarial attacks [6, 9, 10, 24, 43]. Currently, there are two major types of attacks on DNNs. The first is *evasion/adversarial attacks* which cause a *successfully trained* model to misclassify by perturbing the model’s input with imperceptible adversarial noise [9, 27]. The second is *Trojan/backdoor attacks* in which attackers *interfere with the training process* of a model in order to insert hidden malicious features (referred to as *Trojans/backdoors*) into the model [3, 10, 24, 40]. These Trojans do not cause any harm to the model under normal conditions. However, once they are triggered, they will force the model to output the target classes specified by the attackers. Unfortunately, only the attackers know exactly the Trojan triggers and the target classes. Such stealthiness makes Trojan attacks difficult to defend against.

In this work, we focus on defending against Trojan attacks. Most existing Trojan defenses assume that attacks use only *one input-agnostic* Trojan trigger and/or target only *one* class [2, 4, 7, 11, 12, 47]. By constraining the space of possible triggers, these defenses are able to find the true trigger of some simple Trojan attacks satisfying their assumptions [3, 10] and mitigate the attacks. However, these defenses often do not perform well against other advanced attacks that use *multiple input-specific* Trojan triggers and/or target *multiple* classes [5, 31, 32]. In fact, Trojan triggers and attack targets can come in arbitrary numbers and forms only limited by the creativity of attackers. *Thus, it is unrealistic to make assumptions about Trojan triggers and attack targets.*

We advocate general defenses that make no such assumptions and propose two novel defenses of this kind named *Variational Input Filtering (VIF)* and *Adversarial Input Filtering (AIF)*. Both defenses aim at learning a filter  $F$  that can purify all Trojan triggers in the model’s input at run time, hence, are referred to as “*filtering*” defenses. VIF treats  $F$  as a variational autoencoder (VAE) [17] and utilizes the lossy compression property of VAE to discard all noisy informa-

\*The corresponding author

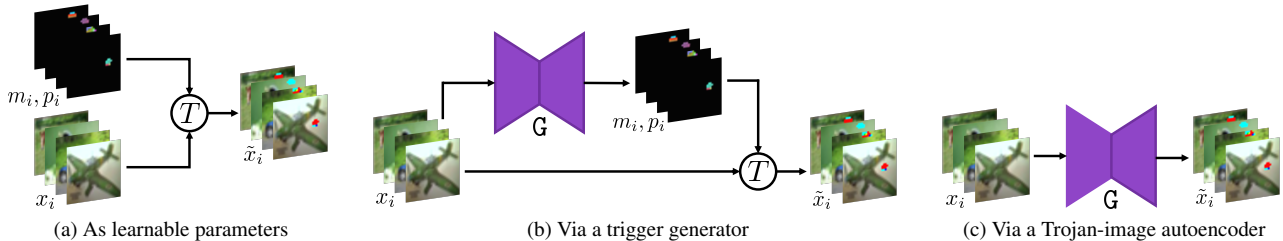


Figure 1: Illustrations of three approaches to model input-specific Trojan triggers  $\psi_i = (m_i, p_i)$  w.r.t.  $x_i$ .

tion in the input including triggers. AIF, on the other hand, uses an auxiliary generator  $G$  to reveal hidden triggers in the input and applies adversarial training [8] to both  $G$  and  $F$  to ensure that  $F$  has removed all potential triggers. In addition, to overcome an issue that input filtering may hurt the model’s prediction on clean data, we introduce a new defense mechanism called “*filtering-then-contrasting*” (*FtC*). The key idea behind FtC is comparing the two outputs of the model with and without input filtering to determine whether the input is clean or not. If the input is marked as clean, the output without input filtering will be used as the final prediction, otherwise, further investigation of the input is required. We equip VIF and AIF with FtC to arrive at the two defenses dubbed VIFtC and AIFtC respectively. Through extensive experiments and ablation studies on different datasets, we demonstrate that our proposed defenses are much more effective and robust than many well-known defenses [4, 7, 21, 47] against a wide range of Trojan attacks including the current state-of-the-art (SOTA) which are Input-Aware Attack [31] and WaNet [32].

## 2. Standard Trojan Attacks

We consider image classification as the task of interest. We denote by  $\mathbb{I}$  the real interval  $[0, 1]$ . In standard Trojan attack scenarios [3, 10], an attacker (usually a service provider) *fully controls* the training process of an image classifier  $C: \mathcal{X} \rightarrow \mathcal{Y}$  where  $\mathcal{X} \subset \mathbb{I}^{c \times h \times w}$  is the input image domain, and  $\mathcal{Y} = \{0, \dots, K-1\}$  is the set of  $K$  classes. The attacker’s goal is to insert a *Trojan* into the classifier  $C$  so that given an input image  $x \in \mathcal{X}$ ,  $C$  will misclassify  $x$  as belonging to a target class  $t \in \mathcal{Y}$  specified by the attacker if  $x$  contains the *Trojan trigger*  $\psi$ , and will predict the true label  $y \in \mathcal{Y}$  of  $x$  otherwise. A common attack strategy to achieve this goal is by poisoning a small portion of the training data with the Trojan trigger  $\psi$ . At each training step, the attacker randomly replaces each clean training pair  $(x, y)$  in the current mini-batch by a poisoned one  $(\tilde{x}, t)$  with a probability  $\rho$  ( $0 < \rho < 1$ ) and trains  $C$  as normal using the modified mini-batch.  $\tilde{x}$  is an image embedded with Trojan triggers (or *Trojan image* for short) corresponding to  $x$ .  $\tilde{x}$  is constructed by combining  $x$  with  $\psi$  via a Trojan injection function  $T(x, \psi)$ . The most common choice of  $T$  is the

image blending function [3, 10] described as follows:

$$\tilde{x} = T(x, \psi) = (1 - m) \odot x + m \odot p, \quad (1)$$

where  $\psi \triangleq (m, p)$ ,  $m \in \mathbb{I}^{c \times h \times w}$  is the trigger mask,  $p \in \mathbb{I}^{c \times h \times w}$  is the trigger pattern, and  $\odot$  is the element-wise product. To ensure  $\tilde{x}$  cannot be detected by human inspection at test time,  $\|m\|$  must be small. Some recent works use more advanced variants of  $T$  such as reflection [23] and warping [32] to craft better natural-looking Trojan images.

Once trained, the Trojan-infected classifier  $C$  will be provided to victims (usually end-users) for deployment. When the victims test  $C$  with their own clean data, they do not see any abnormalities in performance because the Trojan remains dormant for the clean data. Thus, the victims naively believe that  $C$  is normal and use  $C$  as it is without any modification or additional safeguard.

## 3. Difficulty in Finding Input-Specific Triggers

In practice, we (the victims) usually have a small dataset  $\mathcal{D}_{\text{val}} = \{(x_i, y_i)\}_{i=1}^{N_{\text{val}}}$  containing only clean samples for evaluating the performance of  $C$ . We can leverage this set to find possible Trojan triggers associated with the target class  $t$ . For standard Trojan attacks [3, 10] that use only a global *input-agnostic* trigger  $\psi = (m, p)$ ,  $\psi$  can be restored by minimizing the following loss w.r.t.  $m$  and  $p$ :

$$\mathcal{L}_{\text{gen}}(x, t) = -\log p_C(t|\tilde{x}) + \lambda_0 \max(\|m\| - \delta, 0), \quad (2)$$

where  $(x, \cdot) \sim \mathcal{D}_{\text{val}}$ ,  $\tilde{x}$  is derived from  $x$  via Eq. 1,  $p_C(t|\tilde{x}) = \frac{\exp(C_t(\tilde{x}))}{\sum_{k=1}^K \exp(C_k(\tilde{x}))}$  is the probability of  $\tilde{x}$  belonging to the target class  $t$ ,  $\|\cdot\|$  denotes a L1/L2 norm,  $\delta \geq 0$  is an upper bound of the norm, and  $\lambda_0 \geq 0$  is a coefficient. The second term in Eq. 2 ensures that the trigger is small enough so that it could not be detected by human inspection.  $\mathcal{L}_{\text{gen}}$  was used by Neural Cleanse (NC) [47] and its variants [2, 11, 12], and was shown to work well for standard attacks.

In this work, we however consider finding the triggers of Input-Aware Attack (InpAwAtk) [31]. This is a much harder problem because InpAwAtk uses different triggers  $\psi_i = (m_i, p_i)$  for different input images  $x_i$  instead of a global one (Fig. 2c). We examine 3 different ways to model

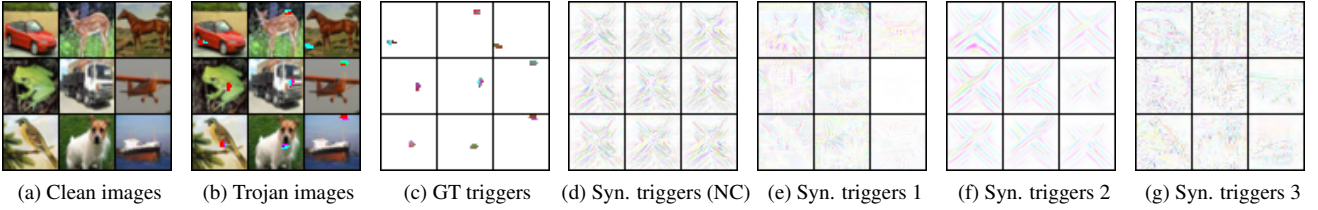


Figure 2: Ground-truth triggers of an Input-Aware Attack (c) corresponding to the clean images in (a). Triggers synthesized by Neural Cleanse (NC) (d) and by the three approaches in Fig. 1 (e, f, g). Trigger pixels are inverted for better visualization.

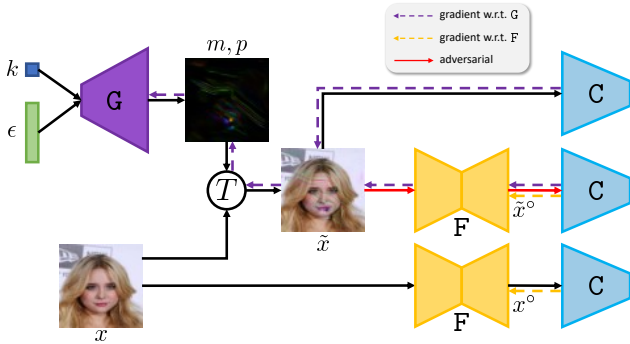


Figure 3: An illustration of Adversarial Input Filtering.

$\psi_i$ : (i) treating  $m_i, p_i$  as learnable parameters for each image  $x_i \in \mathcal{D}_{\text{val}}$ , (ii) via an input-conditional trigger generator  $(m_i, p_i) = G(x_i)$ , and (iii) generating a Trojan image  $\tilde{x}_i$  w.r.t.  $x_i$  via a Trojan-image generator  $\tilde{x}_i = G(x_i)$  and treating  $\tilde{x}_i - x_i$  as  $\psi_i$ . These are illustrated in Fig. 1. The first way does not generalize to other images not in  $\mathcal{D}_{\text{val}}$  while the second and third do. We reuse the loss  $\mathcal{L}_{\text{gen}}$  in Eq. 2 to learn  $m_i, p_i$  in the first way and  $G$  in the second way. The loss to train  $G$  in the third way is slightly adjusted from  $\mathcal{L}_{\text{gen}}$  with  $\|m\|$  replaced by  $\|\tilde{x} - x\|$ . As shown in Fig. 2, neither NC nor the above approaches can restore the original triggers of InpAwAtk, suggesting a new approach is on demand.

## 4. Proposed Trojan Defenses

The great difficulty in finding correct input-specific triggers (Section 3) challenges a majority of existing Trojan defenses which assume a global input-agnostic trigger is applied to all input images [2, 7, 12, 21, 22, 34, 47]. In real-world scenarios, Trojan triggers may come in arbitrary numbers and forms. Thus, it is impractical and almost impossible to find all triggers corresponding to the Trojans in  $\mathcal{C}$ . This raises concern about whether we can effectively defend against various Trojan attacks without making any assumption about triggers. We propose two intuitive solutions to this problem. Both aim at learning a filter  $F$  that can erase most triggers embedded in the input regardless of what they are. Specifically,  $F$  takes an input image  $x$  and computes the

filtered output  $x^\circ$  which serves as input to  $\mathcal{C}$  instead of  $x$ . To be effective,  $x^\circ$  should satisfy the two conditions below:

- *Condition 1*: If  $x$  is clean,  $x^\circ$  should look similar to  $x$  and should have the same label as  $x$ 's. This ensures a *high classification accuracy on clean images* (dubbed “clean accuracy”).
- *Condition 2*: If  $\tilde{x}$  contains triggers,  $\tilde{x}^\circ$  should be close to  $x$  and should have the same label as  $x$ 's where  $x$  is the clean counterpart of  $\tilde{x}$ . This ensures a *low attack success rate* and a *high clean-label recovery rate on Trojan images* (dubbed “Trojan accuracy” and “recovery accuracy”, respectively).

### 4.1. Variational Input Filtering

A natural choice for  $F$  is an autoencoder (AE) which should be complex enough so that  $F$  can reconstruct clean images well to achieve high clean accuracy. However, if  $F$  is too complex, it can capture every detail of a Trojan image including the embedded triggers, which also causes high Trojan accuracy. In general, an optimal  $F$  should achieve good balance between preserving class-related information and discarding noisy information of the input. To reduce the dependence of  $F$  on architecture, we propose to treat  $F$  as a variational autoencoder (VAE)<sup>1</sup> [17] and train it with the “Variational Input Filtering” (VIF) loss given below:

$$\mathcal{L}_{\text{VIF}}(x, y) = -\log p_{\mathcal{C}}(y|x^\circ) + \lambda_1 \|x^\circ - x\| + \lambda_2 D_{\text{KL}}(q(z|x)||p(z)) \quad (3)$$

$$= \mathcal{L}_{\text{IF}} + \lambda_2 D_{\text{KL}}(q(z|x)||p(z)), \quad (4)$$

where  $(x, y) \sim \mathcal{D}_{\text{val}}$ ,  $x^\circ = F(x)$  is the filtered output of  $x$ ,  $z$  is the latent variable of  $x$  computed via the encoder of  $F$ ,  $p(z) = \mathcal{N}(0, I)$  is the standard Gaussian distribution,  $\lambda_1, \lambda_2 \geq 0$ . In Eq. 3, the first two terms force  $F$  to preserve class-related information of  $x$  and to reduce the visual dissimilarity between  $x^\circ$  and  $x$  as per conditions 1, 2 while the last term encourages  $F$  to discard all noisy information of  $x$ . The first two terms constitute the “Input Filtering” (IF)

<sup>1</sup>Denoising Autoencoder (DAE) [46] is also a possible choice but is quite similar to VAE in terms of idea so we do not consider it here.

loss. To the best of our knowledge, IF has not been proposed in other Trojan defense works. Input Processing (IP) [24] is the closest to IF but it is trained on *unlabeled data* using *only the reconstruction loss* (the second term in Eq. 3). In Appdx. A.11.1, we show that IP performs worse than IF, which highlights the importance of the term  $-\log p_C(y|x^\circ)$ .

## 4.2. Adversarial Input Filtering

IF and VIF, owing to their simplicity and universality, do not make use of any Trojan-related knowledge in  $\mathcal{C}$  to train  $F$ . We argue that if  $F$  is exposed to such knowledge,  $F$  could be more selective in choosing which input information to discard, and hence, could perform better. This motivates us to use synthesized Trojan images as additional training data for  $F$  besides clean images from  $\mathcal{D}_{\text{val}}$ . We synthesize a Trojan image  $\tilde{x}$  from a clean image  $x$  as follows:

$$(m_k, p_k) = G(\epsilon, k), \quad (5)$$

$$\tilde{x} = T(x, (m_k, p_k)), \quad (6)$$

where  $G$  is a parameterized generator,  $\epsilon \sim \mathcal{N}(0, I)$  is a standard Gaussian noise,  $k$  is a class label uniformly sampled from  $\mathcal{Y}$ ,  $T$  is the image blending function (Eqs. 1). Since we have no prior knowledge about the target class, we generate Trojan triggers for all classes by making  $G$  conditioned on  $k$ . To make sure that the synthesized Trojan images are useful for  $F$ , we *form an adversarial game between  $G$  and  $F$*  in which  $G$  attempts to generate harder and harder Trojan images that can fool  $F$  into producing the target class (sampled randomly from  $\mathcal{Y}$ ) while  $F$  becomes more robust by correcting these images. We train  $G$  with the following loss:

$$\mathcal{L}_{\text{AIF-gen}}(x, k) = \mathcal{L}_{\text{gen}}(x, k) - \lambda_3 \log p_C(k|\tilde{x}^\circ), \quad (7)$$

where  $\mathcal{L}_{\text{gen}}$  is similar to the one in Eq. 2 but with  $m$  replaced by  $m_k$  (Eq. 5),  $\tilde{x}^\circ = F(\tilde{x})$ ,  $\lambda_3 \geq 0$ . The loss of  $F$  must conform to conditions 1, 2 and is:

$$\begin{aligned} \mathcal{L}_{\text{AIF}}(x, y) &= \mathcal{L}_{\text{IF}}(x, y) - \lambda_4 \log p_C(y|\tilde{x}^\circ) \\ &\quad + \lambda_5 \|\tilde{x}^\circ - x\| \end{aligned} \quad (8)$$

$$= \mathcal{L}_{\text{IF}}(x, y) + \mathcal{L}'_{\text{IF}}(\tilde{x}, y), \quad (9)$$

where AIF stands for “Adversarial Input Filtering”,  $\mathcal{L}_{\text{IF}}$  was described in Eq. 4,  $\tilde{x}$  is computed from  $x$  via Eq. 6,  $\lambda_4, \lambda_5 \geq 0$ . Note that the last term in Eq. 9 is the reconstruction loss between  $\tilde{x}^\circ$  and  $x$  (not  $\tilde{x}$ ). Thus, we denote the last two terms in Eq. 8 as  $\mathcal{L}'_{\text{IF}}$  instead of  $\mathcal{L}_{\text{IF}}$ . AIF is depicted in Fig. 3.

During experiment, we observed that sometimes training  $G$  and  $F$  with the above losses does not result in good performance. The reason is that when  $F$  becomes better,  $G$  tends to produce larger triggers to fool  $F$  despite the fact that a regularization was applied to the norms of these triggers. Too large triggers make learning  $F$  harder as  $\tilde{x}$  is no longer close to  $x$ . To handle this problem, we explicitly normalize  $m_k$  so that its norm is always bounded by  $\delta$ . Details about this technique is given in Appdx. A.12.

## 4.3. Filtering-then-Contrasting Defenses

VIF and AIF always filter  $x$  regardless of whether  $x$  contains triggers or not, which often leads to the decrease in clean accuracy after filtering. To overcome this drawback, we introduce a new defense mechanism called “Filtering then Contrasting” (FtC) which works as follows: Instead of just computing the predicted label  $\hat{y}^\circ$  of the filtered image  $x^\circ = F(x)$  and treat it as the final prediction, we also compute the predicted label  $\hat{y}$  of  $x$  without filtering and compare  $\hat{y}$  with  $\hat{y}^\circ$ . If  $\hat{y}$  is different from  $\hat{y}^\circ$ ,  $x$  is likely to contain triggers and will be alerted for further investigation. Otherwise,  $x$  is marked as clean and  $\hat{y}$  will be used as the final prediction. We derive two new defenses VIFtC and AIFtC from VIF and AIF respectively under this mechanism.

## 5. Experiments

### 5.1. Experimental Setup

**Datasets** Following previous works [10, 31, 37], we evaluate our proposed defenses on 4 image datasets namely MNIST, CIFAR10 [18], GTSRB [41], and CelebA [25]. For CelebA, we follow Salem et al. [37] and select the top 3 most balanced binary attributes (out of 40) to form an 8-class classification problem. The chosen attributes are “Heavy Makeup”, “Mouth Slightly Open”, and “Smiling”. Like other works [7, 47], we assume that we have access to the test set of these datasets. We use 70% data of the test set for training our defense methods ( $\mathcal{D}_{\text{val}}$  in Sections 3, 4) and 30% for testing (denoted as  $\mathcal{D}_{\text{test}}$ ). For more details about the datasets, please refer to Appdx. A.2. Sometimes, we do not test our methods on all images in  $\mathcal{D}_{\text{test}}$  but only on those *not* belonging to the target class. This set is denoted as  $\mathcal{D}'_{\text{test}}$ .

**Attacks** We use 5 different Trojan attacks as test beds for our defenses, which are BadNet+, noise-BI+, image-BI+, InpAwAtk [31], and WaNet [32]. InpAwAtk and WaNet are the current SOTA that were shown to break many strong defenses completely. *To the best of our knowledge, there is currently no effective defense against these two attacks.* BadNet+, noise-BI+, and image-BI+ are variants of BadNet [10] and Blended Injection (BI) [3] that use multiple triggers instead of one. They are analyzed in Appdx. A.10. The training settings for the 5 attacks are given in Appdx. A.3.

We also consider 2 attack modes namely *single-target* and *all-target* [31, 51]. In the first mode, only one class  $t$  is chosen as target. Every Trojan image  $\tilde{x}$  is classified as  $t$  regardless of the ground-truth label of its clean counterpart  $x$ . Without loss of generality,  $t$  is set to 0. In the second mode,  $\tilde{x}$  is classified as  $(k+1) \bmod K$  if  $x$  belongs to the class  $k$ . If not clearly stated, attacks are assumed to be *single-target*.

We report the test clean and Trojan accuracies of the 5 attacks (in single-target mode) in Table 1. It is clear that

Dataset	Benign	BadNet+		noise-BI+		image-BI+		InpAwAtk			WaNet		
	Clean	Clean	Trojan	Clean	Trojan	Clean	Trojan	Clean	Trojan	Cross	Clean	Trojan	Noise
MNIST	99.56	99.61	99.96	99.46	100.0	99.50	100.0	99.47	99.41	96.05	99.48	98.73	99.38
CIFAR10	94.82	94.88	100.0	94.69	100.0	95.15	99.96	94.58	99.43	88.68	94.32	99.59	92.58
GTSRB	99.72	99.34	100.0	99.30	100.0	99.18	100.0	98.90	99.54	95.19	99.12	99.54	99.03
CelebA	79.12	79.41	100.0	78.75	100.0	78.81	99.99	78.18	99.93	77.16	78.48	99.94	77.24

Table 1: Test clean and Trojan accuracies of various Trojan attacks on different datasets.

the attacks achieve very high Trojan accuracies with little or no decrease in clean accuracy compared to the benign model’s, hence, are qualified for our experimental purpose. For results of the attacks on  $\mathcal{D}_{\text{test}}$ , please refer to Appdx. A.5. We also provide results of all-target attacks in Appdx. A.8.

**Baseline defenses** We consider 4 well-known baseline defenses namely Neural Cleanse (NC) [47], STRIP [7], Network Pruning (NP) [21], and Februus [4]. NC assumes that attacks (i) choose only one target class  $t$  and (ii) use *at least* (not exactly) one input-agnostic trigger associated with  $t$ . We refer to (i) as the “*single target class*” assumption and (ii) as the “*input-agnostic trigger*” assumption. Based on these assumptions, NC finds a trigger  $\psi_k = (m_k, p_k)$  for every class  $k \in \mathcal{Y}$  via reverse-engineering (Eq. 2), and uses the L1 norms of the synthesized trigger masks  $\{m_1, \dots, m_K\}$  to detect the target class. The intuition is that if  $t$  is the target class,  $\|m_t\|_1$  will be much smaller than the rest. A  $z$ -value of each mask norm is calculated via Median Absolute Deviation and the  $z$ -value of the smallest mask norm (referred to as the *anomaly index*) is compared against a threshold  $\zeta$  (2.0 by default). If the anomaly index is smaller than  $\zeta$ ,  $\mathcal{C}$  is marked as clean. Otherwise,  $\mathcal{C}$  is marked Trojan-infected with the target class corresponding to the smallest mask norm. In this case, the Trojans in  $\mathcal{C}$  can be mitigated via pruning or via checking the cleanliness of input images. Both mitigation methods make use of  $\psi_t$  and are analyzed in Appdx. A.6.

STRIP assumes triggers are input-agnostic and argues that if an input image  $x$  contains triggers then these triggers still have effect if  $x$  is superimposed (blended) with other images. Therefore, STRIP superimposes  $x$  with  $N_s$  random clean images from  $\mathcal{D}_{\text{val}}$  and computes the *average entropy*  $\mathcal{H}(x)$  of  $N_s$  predicted class probabilities corresponding to  $N_s$  superimposed versions of  $x$ . If  $\mathcal{H}(x)$  is smaller than a threshold  $\tau$ ,  $x$  is considered as trigger-embedded, otherwise, clean.  $\tau$  is set according to the false positive rate (FPR) over the average entropies of all images in  $\mathcal{D}_{\text{val}}$ , usually at FPR = 1/5/10%. We evaluate the performance of STRIP against an attack using  $M_s$  random clean images from  $\mathcal{D}_{\text{test}}$  and  $M_s$  corresponding Trojan images generated by that attack. Following [7], we set  $N_s = 100$  and  $M_s = 2000$ .

Network Pruning (NP) hypothesizes that idle neurons are more likely to store Trojan-related information. Thus, it

ranks neurons in the second top layer<sup>2</sup> of  $\mathcal{C}$  according to their average activation over all clean images in  $\mathcal{D}_{\text{val}}$  and gradually prunes them until a certain decrease in clean accuracy is reached, usually at 1/5/10%.

Among the 4 baselines, Februus is the most related to our filtering defenses since it mitigates Trojan attacks via input purification. It uses GradCAM [39] to detect regions in an input image  $x$  that may contain triggers. Then, it removes all pixels in the suspected regions and generates new ones via inpainting. The inpainted image is expected to contain no trigger and is sent to  $\mathcal{C}$  to predict as normal.

**Model architectures, training settings** Please refer to Appdx. A.4 for more detail.

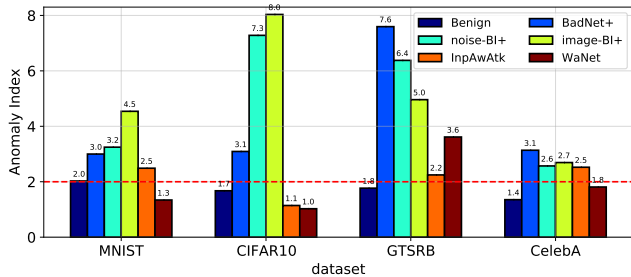
**Metrics** We evaluate VIF/AIF using 3 metrics namely *decrease in clean accuracy* ( $\downarrow\mathcal{C}$ ), *Trojan accuracy* (T), and *decrease in recovery accuracy* ( $\downarrow\mathcal{R}$ ). The first is the difference between the classification accuracies of clean images before and after filtering. The second is the attack success rate of Trojan images after filtering. The last is the difference between the classification accuracy of clean images before filtering and that of the corresponding Trojan images after filtering. *For all the 3 metrics, lower values are better.*  $\downarrow\mathcal{C}$  and  $\downarrow\mathcal{R}$  are computed on  $\mathcal{D}_{\text{test}}$ . T is computed on  $\mathcal{D}'_{\text{test}}$  under single-target attacks and  $\mathcal{D}_{\text{test}}$  under all-target attacks. This ensures that T can be 0 in the best case. Otherwise, T will be around  $1/K$  where  $K$  is the total number of classes.  $\downarrow\mathcal{C}$  and  $\downarrow\mathcal{R}$  are upper-bounded by 1 and can be negative.

We evaluate VIFtC/AIFtC using FPR and FNR. FPR/FNR is defined as the proportion of clean/Trojan images having different/similar class predictions when the filter  $F$  is applied and not applied. FPR is computed on  $\mathcal{D}_{\text{test}}$ . FNR is computed on  $\mathcal{D}'_{\text{test}}$  under single-target attacks and  $\mathcal{D}_{\text{test}}$  under all-target attacks. Both metrics are in  $[0, 1]$  and smaller values of them are better. Interestingly, FPR and FNR are strongly correlated to  $\downarrow\mathcal{C}$  and T, respectively. FPR/FNR is exactly equal to  $\downarrow\mathcal{C}/T$  if  $\mathcal{C}$  achieves perfect clean/Trojan accuracy.

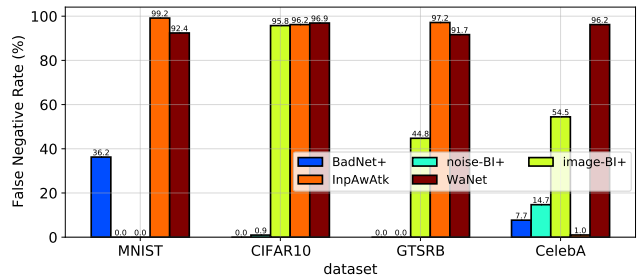
## 5.2. Results of Baseline Defenses

In Fig. 4, we show the detection results of Neural Cleanse (NC) and STRIP w.r.t. the aforementioned attacks. The two defenses are effective against BadNet+ and image/noise-BI+.

<sup>2</sup>the one before the softmax layer



(a) Neural Cleanse



(b) STRIP

Figure 4: (a) Anomaly indices of Neural Cleanse. The red dashed line indicates the threshold. (b) FNRs of STRIP at 10% FPR.

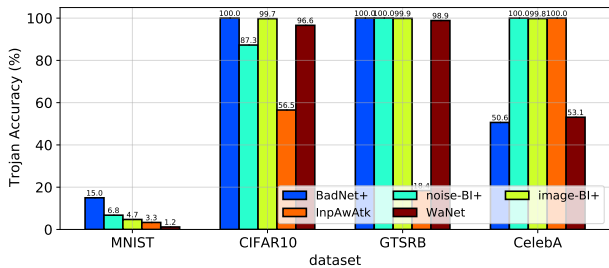
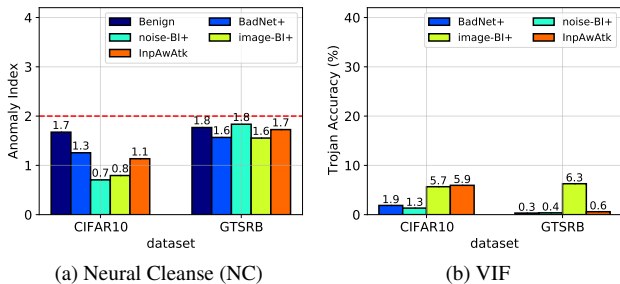


Figure 5: Trojan accuracies at 10% decrease in clean accuracy of different Trojan models pruned by Network Pruning.



(a) Neural Cleanse (NC)

(b) VIF

Figure 6: Anomaly indices of NC (a) and Trojan accuracies of VIF (b) against different Trojan attacks. We only show results on CIFAR10 and GTSRB due to space limit.

This is because STRIP and NC generally do not make any assumption about the number of triggers. However, STRIP performs poorly against InpAwAtk and WaNet (FNRs > 90%) since these advanced attacks break its “input-agnostic trigger” assumption. NC also fails to detect the Trojan classifiers trained by WaNet on most datasets for the same reason. What surprises us is that in our experiment NC correctly detect the Trojan classifiers trained by InpAwAtk on 3/4 datasets while in the original paper [31], it was shown to fail completely. We are confident that this inconsistency does not come from our implementation of InpAwAtk since we used the same

hyperparameters and achieved the same classification results as those in the original paper (Table 1 versus Fig. 3b in [31]). However, NC is still unable to mitigate all Trojans in these correctly-detected Trojan classifiers (Appdx. A.6.3). In addition, as shown in Fig. 6a, NC is totally vulnerable to *all-target attacks* since its “single target class” assumption is no longer valid under these attacks. Network Pruning (NP), despite being assumption-free, cannot mitigate Trojans from most attacks (high Trojan accuracies in Fig. 5) as it fails to prune the correct neurons containing Trojans. Februs has certain effects on mitigating Trojans from BadNet+ while being useless against the remaining attacks (high Ts in Table 2). This is because GradCAM, the method used by Februs, is only suitable for detecting patch-like triggers of BadNet+, not full-size noise-like triggers of image/noise-BI+ or polymorphic triggers of InpAwAtk/WaNet. We also observe that Februs significantly reduces the clean accuracy (high  $\downarrow C$ s in Table 2) as it removes input regions that contain no Trojan trigger yet are highly associated with the output class. This problem, however, was not discussed in the Februs paper. We encourage readers to check Appdx. A.6 for more results of the baseline defenses.

### 5.3. Results of Proposed Defenses

From Table 2, it is clear that VIF and AIF achieve superior performances in mitigating Trojans of all the attacks compared to the baseline defenses. For example, on MNIST and GTSRB, our filtering defenses impressively reduce T from about 100% (Table 1) to less than 2% for most attacks yet only cause less than 1% drop of clean accuracy ( $\downarrow C < 1\%$ ). On more diverse datasets such as CIFAR10 and CelebA, VIF and AIF still achieve T less than 6% and 12% for most attacks while maintaining  $\downarrow C$  below 8% and 5%, respectively. We note that on CelebA, the nonoptimal performance of C (accuracy  $\approx 79\%$ ) makes T higher than normal because T may contains the error of samples from non-target classes misclassified as the target class. However, it is not trivial to disentangle the two quantities so we leave this problem for future work. As there is no free lunch, our

Dataset	Defense	Benign	BadNet+			noise-BI+			image-BI+			InpAwAtk			WaNet		
		↓C	↓C	T	↓R	↓C	T	↓R	↓C	T	↓R	↓C	T	↓R	↓C	T	↓R
MNIST	Feb.	5.96	39.08	96.24	86.32	2.30	100.0	89.58	8.19	100.0	89.58	9.90	92.40	83.32	25.43	80.46	88.75
	IF	<b>0.10</b>	0.27	2.47	4.99	<b>0.10</b>	0.16	13.52	0.13	1.29	12.02	0.21	<b>0.96</b>	2.08	0.23	0.34	0.61
	VIF	0.13	<b>0.17</b>	<b>2.36</b>	<b>3.63</b>	0.12	<b>0.04</b>	0.63	<b>0.03</b>	<b>0.11</b>	0.40	0.20	1.25	1.83	<b>0.10</b>	0.48	0.53
	AIF	<b>0.10</b>	<b>0.17</b>	3.80	4.86	0.13	0.15	<b>0.11</b>	0.10	<b>0.11</b>	<b>0.10</b>	<b>0.03</b>	1.14	<b>1.66</b>	0.13	<b>0.15</b>	<b>0.20</b>
CIFAR10	Feb.	32.67	49.17	12.63	19.57	26.73	43.59	78.90	39.70	92.67	81.00	53.43	49.52	66.50	55.80	98.70	83.30
	IF	<b>3.34</b>	<b>4.15</b>	<b>2.30</b>	<b>7.79</b>	<b>3.32</b>	<b>1.01</b>	<b>4.43</b>	<b>4.76</b>	37.48	34.30	<b>4.47</b>	16.35	18.96	<b>3.21</b>	4.82	6.80
	VIF	7.81	7.70	2.52	11.27	6.43	1.22	7.10	7.53	10.52	16.50	7.67	<b>3.07</b>	12.38	7.97	3.96	10.67
	AIF	4.67	5.60	2.37	9.03	4.87	1.14	6.02	5.23	<b>1.96</b>	<b>7.10</b>	5.28	5.30	<b>11.87</b>	4.30	<b>1.22</b>	<b>5.67</b>
GTSRB	Feb.	42.01	35.30	21.02	44.11	43.40	75.75	95.90	32.18	97.83	97.37	21.27	70.02	72.71	33.18	70.10	71.69
	IF	0.12	0.13	<b>0.00</b>	2.55	0.13	0.03	1.52	0.37	52.27	51.95	0.03	0.66	3.60	0.08	9.83	9.62
	VIF	0.18	0.45	<b>0.00</b>	3.55	0.18	<b>0.00</b>	1.12	0.37	12.12	16.56	0.11	<b>0.03</b>	1.87	0.55	3.67	3.89
	AIF	<b>0.05</b>	<b>-0.16</b>	<b>0.00</b>	<b>1.87</b>	<b>0.05</b>	<b>0.00</b>	<b>0.81</b>	<b>0.13</b>	<b>7.47</b>	<b>9.54</b>	<b>-0.03</b>	0.05	<b>1.37</b>	<b>-0.05</b>	<b>0.50</b>	<b>0.42</b>
CelebA	Feb.	12.71	18.80	42.96	21.33	11.76	93.27	49.05	13.30	98.59	49.84	5.60	99.98	49.71	9.16	97.30	48.53
	IF	<b>2.23</b>	<b>4.21</b>	8.62	<b>4.75</b>	<b>2.57</b>	13.83	6.00	<b>2.25</b>	59.39	27.94	<b>2.86</b>	11.95	<b>6.07</b>	<b>2.43</b>	15.21	4.75
	VIF	3.74	4.63	9.28	4.90	3.20	<b>11.51</b>	<b>4.08</b>	3.54	<b>14.32</b>	<b>5.62</b>	3.89	11.55	6.27	3.96	<b>8.30</b>	<b>4.19</b>
	AIF	4.95	6.46	<b>7.85</b>	6.49	4.18	12.56	6.52	4.37	18.40	9.23	3.71	<b>10.43</b>	7.65	4.02	12.82	5.74

Table 2: Trojan filtering results (in %) of Februus (Feb.) and our filtering defenses against different Trojan attacks on different datasets. For a particular dataset, attack, and metric, the best among the 4 defenses are highlighted in bold.

Dataset	Defense	InpAwAtk		WaNet	
		FPR	FNR	FPR	FNR
CIFAR10	IFtC	<b>7.25</b>	16.89	<b>7.17</b>	5.15
	VIFtC	10.63	<b>3.67</b>	11.40	4.26
	AIFtC	8.27	5.93	7.93	<b>1.56</b>
GTSRB	IFtC	<b>0.29</b>	1.00	0.66	10.41
	VIFtC	0.53	<b>0.37</b>	1.31	4.25
	AIFtC	0.47	0.40	<b>0.60</b>	<b>1.08</b>

Table 3: FPRs and FNRs of VIFtC and AIFtC against InpAwAtk and WaNet on CIFAR10 and GTSRB.

filtering defenses may be not as good as some baselines in some specific cases. For example, on CIFAR10, STRIP achieves FNRs  $\approx 0\%$  against BadNet+/noise-BI+ (Fig. 4b) while VIF/AIF achieves Ts  $\approx 1\text{-}3\%$ . However, the gaps are very small and in general, our filtering defenses are still much more effective than the baseline defenses against all the single-target attacks. Our filtering defenses also perform well against *all-target* attacks (Fig. 6b and Appdx. A.9) as ours are not sensitive to the number of target classes. To gain a better insight into the performance of VIF/AIF, we visualize the filtered images produced by VIF/AIF and their corresponding “counter-triggers” in Appdx. A.14.

Among our filtering defenses, IF usually achieves the smallest  $\downarrow C$ s because its loss does not have any term that encourages information removal like VIF’s and AIF’s. The gaps in  $\downarrow C$  between IF and AIF/VIF are the largest on CIFAR10 but do not exceed 5%. However, IF usually performs much worse than VIF/AIF in mitigating Trojans, especially those from image-BI+, InpAwAtk, and WaNet. For example, on CIFAR10, GTSRB, and CelebA, IF reduces the attack success rate (T) of image-BI+ to 37.48%, 52.27%, and 59.39% respectively. These numbers are only 1.96%, 7.47%, and

18.40% for AIF and 10.52%, 12.12%, and 14.32% for VIF. Therefore, when considering the trade-off between  $\downarrow C$  and T, VIF and AIF are clearly better than IF. We also observe that AIF usually achieves lower  $\downarrow C$ s and  $\downarrow R$ s than VIF. It is because AIF discards only potential malicious information instead of all noisy information like VIF. However, VIF is simpler and easier to train than AIF.

From Table 3, we see that the FPRs and FNRs of VIFtC/AIFtC are close to the  $\downarrow C$ s and Ts of VIF/AIF respectively on CIFAR10 and GTSRB. This is because the Trojan classifier C achieves nearly 100% clean and Trojan accuracies on the two datasets. Thus, we can interpret the results of VIFtC/AIFtC in the same way as what we have done for VIF/AIF. Since FPR only affects the classification throughput not accuracy, VIFtC/AIFtC are preferred to VIF/AIF in applications that favor accuracy. For full results of our FtC defenses, please refer to Appdx. A.7.

## 5.4. Ablation Studies

It is undoubted that our defenses require some settings to work well. However, these settings *cannot be managed by attackers* unlike the assumptions of existing defenses. Due to space limit, below we only analyze one setting. For others, please refer to Appdx. A.11.

### 5.4.1 Different coefficients of the $D_{KL}$ in $\mathcal{L}_{VIF}$

In Fig. 7, we show the performances of VIF w.r.t. different values of  $\lambda_2$  - the coefficient of  $D_{KL}$  in Eq. 3. It is clear that  $\lambda_2$  trades off between clean accuracy (C) and Trojan accuracy (T). Smaller  $\lambda_2$  leads to higher C yet lower T and vice versa. Recovery accuracy (R), to some extent, can be seen as a combination of C and T. Thus, we based on R to decide the optimal value for  $\lambda_2$ . From the results on

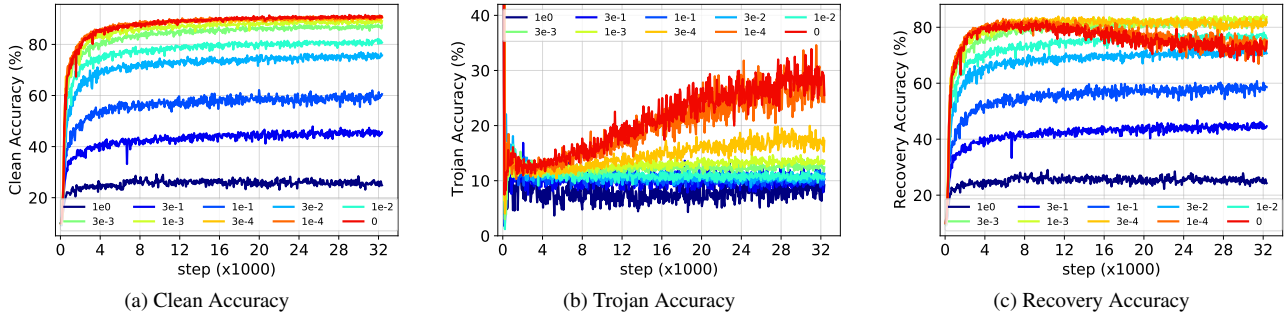


Figure 7: Clean, Trojan, and recovery accuracy curves of VIF against InpAwAtk on CIFAR10 w.r.t. different coefficients of  $D_{KL}$  ( $\lambda_2$  in Eq. 3). The Trojan accuracy curves in (b) fluctuate around 10% since they are computed on  $\mathcal{D}_{test}$  instead of  $\mathcal{D}'_{test}$ .

CIFAR10 (Fig. 7) and on other datasets, we found  $\lambda_2 = 0.003$  to be the best so we set it as default.

## 6. Related Work

Due to space limit, in this section we only discuss related work about Trojan defenses. Related work about Trojan attacks are provided in Appdx. A.1. A large number of Trojan defenses have been proposed so far, among which Neural Cleanse (NC) [47], Network Pruning (NP) [21], STRIP [7], and Februs [4] are representative for 4 different types of defenses and are carefully analyzed in Section 5.1. DeepInspect [2], MESA [34] improve upon NC by synthesizing a distribution of triggers for each class instead of just a single one. TABOR [11] adds more regularization losses to NC to better handle large and scattered triggers. STS [12] restores triggers by minimizing a novel loss function which is the pairwise difference between the class probabilities of two random synthesized Trojan images. This makes STS independent of the number of classes and more efficient than NC on datasets with many classes. ABS [22] is a quite complicated defense inspired by brain stimulation. It analyzes all neurons in the classifier  $C$  to find “compromised” ones and use these neurons to validate whether  $C$  is attacked or not. DL-TND [48], B3D [5] focus on detecting Trojan-infected models in case validation data are limited. However, all the aforementioned defenses derived from NC still make the same “input-agnostic trigger” and “single target class” assumptions as NC, and hence, are supposed to be ineffective against attacks that break these assumptions such as input-aware [31, 32] and all-target attacks. Activation Clustering [1] and Spectral Signatures [44] regard hidden activations as a clue to detect Trojan samples from BadNet [10]. They base on an empirical observation that the hidden activations of Trojan samples and clean samples of the target class usually form distinct clusters in the hidden activation space. These defenses are of the same kind as STRIP and are not applicable to all-target attacks. Mode Connectivity Repair (MCR) [51] and Attention Distillation (AD) [20] belong to the class

of pruning/fine-tuning methods like NP. MCR mitigates Trojans by choosing an interpolated model near the two end points of a parametric path connecting a Trojan model and its fine-tuned version. The path’s parameters are learned using provided clean data. Nguyen et al. [31] applied MCR to InpAwAtk and observed that the corresponding interpolated models have roughly similar clean and Trojan accuracies. It means MCR is not effective against InpAwAtk because if we pick an interpolated model for low Trojan accuracy, this model will have low clean accuracy too. AD regards a fine-tuned Trojan model as a teacher and fine-tunes the original Trojan model again with a so-called “attention distillation” from the teacher. AD was shown to be better than MCR but has only been tested against standard Trojan attacks.

## 7. Conclusion

In this work, we advocated general Trojan defenses that make no assumption about triggers and target classes. We proposed two novel “filtering” defenses with this characteristic dubbed VIF and AIF that leverage variational inference and adversarial learning respectively to effectively purify all potential Trojan triggers embedded in an input. We further extended “filtering” to “filtering-then-contrasting” (FtC) - a new defense mechanism that circumvents the loss in clean accuracy caused by “filtering”. We applied FtC to VIF, AIF to derive VIFtC, AIFtC respectively. Through extensive experiments, we demonstrated that our proposed defenses significantly outperform well-known defenses in mitigating various Trojan attacks including 2 current SOTA. We hope our positive results will inspire future research on general Trojan defenses. We also want to extend our proposed defenses to other domains (e.g., texts, graphs) and other tasks (e.g., object detection, visual reasoning) which we believe are more challenging than the image domain and image classification task considered in this work, respectively.



## 8. Limitations

Besides the advantages presented in the previous sections, our proposed defenses still have the following limitations:

- It is intuitive that our defenses are mainly applicable to attacks that use small-norm<sup>3</sup> triggers. If triggers have too large norms, F is likely unable to completely remove the embedded triggers from input Trojan images and hence, the filtered images outputted by F can still trigger the Trojans in C. However, in practice, it is very unusual for a Trojan attack to use large-norm triggers because the Trojan images will be easily detected via human inspection. We discussed this in Sections 2, 4. We also analyze the robustness of our defenses to big-norm triggers in Appdx. A.11.4.
- Like most other Trojan defenses, our defenses require certain amount of clean training data to achieve good results. This is analyzed in Appdx. A.11.3.
- The performance of our defenses also depends on the architecture of the filter F, which is analyzed in Appdx. A.11.2.
- Our defenses have only been tested on image data. For data from other domains like texts or graphs, our defenses may require some adjustments to work well. We consider this as future work and mentioned in the Conclusion.

## References

- [1] Bryant Chen, Wilka Carvalho, Nathalie Baracaldo, Heiko Ludwig, Benjamin Edwards, Taesung Lee, Ian Molloy, and Biplav Srivastava. Detecting backdoor attacks on deep neural networks by activation clustering. *arXiv preprint arXiv:1811.03728*, 2018. 8
- [2] Huili Chen, Cheng Fu, Jishen Zhao, and Farinaz Koushanfar. DeepInspect: A Black-box Trojan Detection and Mitigation Framework for Deep Neural Networks. In *Proceedings of the 28th International Joint Conference on Artificial Intelligence. AAAI Press*, pages 4658–4664, 2019. 1, 2, 3, 8
- [3] Xinyun Chen, Chang Liu, Bo Li, Kimberly Lu, and Dawn Song. Targeted backdoor attacks on deep learning systems using data poisoning. *arXiv preprint arXiv:1712.05526*, 2017. 1, 2, 4, 12
- [4] Bao Gia Doan, Ehsan Abbasnejad, and Damith C Ranasinghe. Februus: Input purification defense against trojan attacks on deep neural network systems. In *Annual Computer Security Applications Conference*, pages 897–912, 2020. 1, 2, 5, 8
- [5] Yinpeng Dong, Xiao Yang, Zhijie Deng, Tianyu Pang, Zihao Xiao, Hang Su, and Jun Zhu. Black-box detection of backdoor attacks with limited information and data. *arXiv preprint arXiv:2103.13127*, 2021. 1, 8
- [6] Alhussein Fawzi, Hamza Fawzi, and Omar Fawzi. Adversarial vulnerability for any classifier. *arXiv preprint arXiv:1802.08686*, 2018. 1
- [7] Yansong Gao, Change Xu, Derui Wang, Shiping Chen, Damith C Ranasinghe, and Surya Nepal. Strip: A Defence Against Trojan Attacks on Deep Neural Networks. In *Proceedings of the 35th Annual Computer Security Applications Conference*, pages 113–125, 2019. 1, 2, 3, 4, 5, 8
- [8] Ian Goodfellow, Jean Pouget-Abadie, Mehdi Mirza, Bing Xu, David Warde-Farley, Sherjil Ozair, Aaron Courville, and Yoshua Bengio. Generative adversarial nets. *Advances in neural information processing systems*, 27, 2014. 2
- [9] Ian J Goodfellow, Jonathon Shlens, and Christian Szegedy. Explaining and harnessing adversarial examples. *arXiv preprint arXiv:1412.6572*, 2014. 1
- [10] Tianyu Gu, Brendan Dolan-Gavitt, and Siddharth Garg. Badnets: Identifying vulnerabilities in the machine learning model supply chain. *arXiv preprint arXiv:1708.06733*, 2017. 1, 2, 4, 8, 12, 15
- [11] Wenbo Guo, Lun Wang, Xinyu Xing, Min Du, and Dawn Song. Tabor: A highly accurate approach to inspecting and restoring trojan backdoors in ai systems. *arXiv preprint arXiv:1908.01763*, 2019. 1, 2, 8
- [12] H Harikumar, Vuong Le, Santu Rana, S Bhattacharya, Sunil Gupta, and Svetha Venkatesh. Scalable backdoor detection in neural networks. In *Joint European Conference on Machine Learning and Knowledge Discovery in Databases (ECML PKDD)*, pages 289–304. Springer, 2020. 1, 2, 3, 8
- [13] Kaiming He, Xiangyu Zhang, Shaoqing Ren, and Jian Sun. Deep residual learning for image recognition. In *Proceedings of the IEEE conference on computer vision and pattern recognition*, pages 770–778, 2016. 12
- [14] Kaiming He, Xiangyu Zhang, Shaoqing Ren, and Jian Sun. Identity mappings in deep residual networks. In *European conference on computer vision*, pages 630–645. Springer, 2016. 12, 18
- [15] Yujie Ji, Xinyang Zhang, and Ting Wang. Backdoor attacks against learning systems. In *IEEE Conference on Communications and Network Security*, pages 1–9. IEEE, 2017. 12
- [16] Diederik P Kingma and Jimmy Ba. Adam: A Method for Stochastic Optimization. *arXiv preprint arXiv:1412.6980*, 2014. 13

<sup>3</sup>Small-norm triggers is not equivalent to small-size triggers. For example, in noise-BI+/image-BI+, triggers have full sizes yet small norms.

- [17] Diederik P Kingma and Max Welling. Auto-encoding variational bayes. *arXiv preprint arXiv:1312.6114*, 2013. 1, 3
- [18] Alex Krizhevsky. Learning Multiple Layers of Features from Tiny Images. Technical report, 2009. 4
- [19] Yuezun Li, Yiming Li, Baoyuan Wu, Longkang Li, Ran He, and Siwei Lyu. Backdoor attack with sample-specific triggers. *arXiv preprint arXiv:2012.03816*, 2020. 12
- [20] Yige Li, Xixiang Lyu, Nodens Koren, Lingjuan Lyu, Bo Li, and Xingjun Ma. Neural attention distillation: Erasing backdoor triggers from deep neural networks. *arXiv preprint arXiv:2101.05930*, 2021. 8
- [21] Kang Liu, Brendan Dolan-Gavitt, and Siddharth Garg. Fine-pruning: Defending against backdooring attacks on deep neural networks. In *International Symposium on Research in Attacks, Intrusions, and Defenses*, pages 273–294. Springer, 2018. 2, 3, 5, 8, 13
- [22] Yingqi Liu, Wen-Chuan Lee, Guanhong Tao, Shiqing Ma, Yousra Aafer, and Xiangyu Zhang. ABS: Scanning Neural Networks for Back-doors by Artificial Brain Stimulation. In *Proceedings of the ACM SIGSAC Conference on Computer and Communications Security*, pages 1265–1282, 2019. 3, 8
- [23] Yunfei Liu, Xingjun Ma, James Bailey, and Feng Lu. Reflection backdoor: A natural backdoor attack on deep neural networks. In *European Conference on Computer Vision*, pages 182–199. Springer, 2020. 2, 12
- [24] Yuntao Liu, Yang Xie, and Ankur Srivastava. Neural trojans. In *2017 IEEE International Conference on Computer Design (ICCD)*, pages 45–48. IEEE, 2017. 1, 4, 12, 16, 19
- [25] Ziwei Liu, Ping Luo, Xiaogang Wang, and Xiaoou Tang. Deep learning face attributes in the wild. In *Proceedings of the IEEE international conference on computer vision*, pages 3730–3738, 2015. 4
- [26] Christos Louizos, Karen Ullrich, and Max Welling. Bayesian compression for deep learning. *arXiv preprint arXiv:1705.08665*, 2017. 18
- [27] Aleksander Madry, Aleksandar Makelov, Ludwig Schmidt, Dimitris Tsipras, and Adrian Vladu. Towards deep learning models resistant to adversarial attacks. *arXiv preprint arXiv:1706.06083*, 2017. 1
- [28] Pim Moeskops, Mitko Veta, Maxime W Lafarge, Koen AJ Eppenhof, and Josien PW Pluim. Adversarial training and dilated convolutions for brain mri segmentation. In *Deep learning in medical image analysis and multimodal learning for clinical decision support*, pages 56–64. Springer, 2017. 1
- [29] Dmitry Molchanov, Arsenii Ashukha, and Dmitry Vetrov. Variational dropout sparsifies deep neural networks. In *International Conference on Machine Learning*, pages 2498–2507. PMLR, 2017. 18
- [30] Luis Muñoz-González, Bjarne Pfizner, Matteo Russo, Javier Carnerero-Cano, and Emil C Lupu. Poisoning attacks with generative adversarial nets. *arXiv preprint arXiv:1906.07773*, 2019. 12
- [31] Anh Nguyen and Anh Tran. Input-aware dynamic backdoor attack. *arXiv preprint arXiv:2010.08138*, 2020. 1, 2, 4, 6, 8, 12
- [32] Anh Nguyen and Anh Tran. Wanet-imperceptible warping-based backdoor attack. *International Conference on Learning Representations*, 2021. 1, 2, 4, 8, 12
- [33] Omkar M Parkhi, Andrea Vedaldi, and Andrew Zisserman. Deep face recognition. 2015. 1
- [34] Ximing Qiao, Yukun Yang, and Hai Li. Defending neural backdoors via generative distribution modeling. *arXiv preprint arXiv:1910.04749*, 2019. 3, 8
- [35] Joseph Redmon, Santosh Divvala, Ross Girshick, and Ali Farhadi. You only look once: Unified, real-time object detection. In *Proceedings of the IEEE conference on computer vision and pattern recognition*, pages 779–788, 2016. 1
- [36] Aniruddha Saha, Akshayvarun Subramanya, and Hamed Pirsiavash. Hidden trigger backdoor attacks. In *Proceedings of the AAAI Conference on Artificial Intelligence*, volume 34, pages 11957–11965, 2020. 12
- [37] Ahmed Salem, Rui Wen, Michael Backes, Shiqing Ma, and Yang Zhang. Dynamic backdoor attacks against machine learning models. *arXiv preprint arXiv:2003.03675*, 2020. 4, 12
- [38] Florian Schroff, Dmitry Kalenichenko, and James Philbin. Facenet: A unified embedding for face recognition and clustering. In *Proceedings of the IEEE conference on computer vision and pattern recognition*, pages 815–823, 2015. 1
- [39] Ramprasaath R Selvaraju, Michael Cogswell, Abhishek Das, Ramakrishna Vedantam, Devi Parikh, and Dhruv Batra. Grad-cam: Visual explanations from deep networks via gradient-based localization. In *Proceedings of the IEEE international conference on computer vision*, pages 618–626, 2017. 5
- [40] Ali Shafahi, W Ronny Huang, Mahyar Najibi, Octavian Suci, Christoph Studer, Tudor Dumitras, and Tom Goldstein. Poison frogs! targeted clean-label poisoning attacks on neural networks. *arXiv preprint arXiv:1804.00792*, 2018. 1, 12
- [41] Johannes Stallkamp, Marc Schlipsing, Jan Salmen, and Christian Igel. Man vs. Computer: Benchmarking

- Machine Learning Algorithms for Traffic Sign Recognition. *Neural Networks*, pages 323–332, 2012. 4
- [42] Waqas Sultani, Chen Chen, and Mubarak Shah. Real-world anomaly detection in surveillance videos. In *Proceedings of the IEEE conference on computer vision and pattern recognition*, pages 6479–6488, 2018. 1
- [43] Simen Thys, Wiebe Van Ranst, and Toon Goedemé. Fooling automated surveillance cameras: adversarial patches to attack person detection. In *Proceedings of the IEEE/CVF Conference on Computer Vision and Pattern Recognition Workshops*, pages 0–0, 2019. 1
- [44] Brandon Tran, Jerry Li, and Aleksander Madry. Spectral Signatures in Backdoor Attacks. In *Advances in Neural Information Processing Systems*, pages 8000–8010, 2018. 8
- [45] Mart van Baalen, Christos Louizos, Markus Nagel, Rana Ali Amjad, Ying Wang, Tijmen Blankevoort, and Max Welling. Bayesian bits: Unifying quantization and pruning. *arXiv preprint arXiv:2005.07093*, 2020. 18
- [46] Pascal Vincent, Hugo Larochelle, Yoshua Bengio, and Pierre-Antoine Manzagol. Extracting and composing robust features with denoising autoencoders. In *Proceedings of the 25th international conference on machine learning*, pages 1096–1103, 2008. 3
- [47] Bolun Wang, Yuanshun Yao, Shawn Shan, Huiying Li, Bimal Viswanath, Haitao Zheng, and Ben Y Zhao. Neural Cleanse: Identifying and Mitigating Backdoor Attacks in Neural Networks. In *IEEE Symposium on Security and Privacy*, pages 707–723. IEEE, 2019. 1, 2, 3, 4, 5, 8, 12
- [48] Ren Wang, Gaoyuan Zhang, Sijia Liu, Pin-Yu Chen, Jinjun Xiong, and Meng Wang. Practical detection of trojan neural networks: Data-limited and data-free cases. In *Computer Vision—ECCV 2020: 16th European Conference, Glasgow, UK, August 23–28, 2020, Proceedings, Part XXIII 16*, pages 222–238. Springer, 2020. 8
- [49] Emily Wenger, Josephine Passananti, Arjun Nitin Bhagoji, Yuanshun Yao, Haitao Zheng, and Ben Y Zhao. Backdoor attacks against deep learning systems in the physical world. In *Proceedings of the IEEE/CVF Conference on Computer Vision and Pattern Recognition*, pages 6206–6215, 2021. 12
- [50] Dong Yang, Daguang Xu, S Kevin Zhou, Bogdan Georgescu, Mingqing Chen, Sasa Grbic, Dimitris Metaxas, and Dorin Comaniciu. Automatic liver segmentation using an adversarial image-to-image network. In *International Conference on Medical Image Computing and Computer-Assisted Intervention*, pages 507–515. Springer, 2017. 1
- [51] Pu Zhao, Pin-Yu Chen, Payel Das, Karthikeyan Natesan Ramamurthy, and Xue Lin. Bridging mode connectivity in loss landscapes and adversarial robustness. *arXiv preprint arXiv:2005.00060*, 2020. 4, 8
- [52] Chen Zhu, W Ronny Huang, Hengduo Li, Gavin Taylor, Christoph Studer, and Tom Goldstein. Transferable clean-label poisoning attacks on deep neural nets. In *International Conference on Machine Learning*, pages 7614–7623. PMLR, 2019. 12

## Table of Content for Appendix

<b>A Appendix</b>	<b>12</b>
A.1. Related Work about Trojan Attacks . . . . .	12
A.2 Datasets . . . . .	12
A.3. Model Architectures and Training Settings for the Attacks . . . . .	12
A.4. Model Architectures, Training Settings, and Metrics for our Defenses . . . . .	13
A.5. Results of the Attacks on $\mathcal{D}_{\text{test}}$ . . . . .	13
A.6 Full Results of the Baseline Defenses . . . . .	13
A.7. Full Results of Our FtC Defenses . . . . .	15
A.8 Results of All-target Attacks . . . . .	15
A.9. Results of Our Proposed Defenses against All-target Attacks . . . . .	15
A.10 BadNet+ and Noise/Image-BI+ . . . . .	15
A.1.1 Additional Ablation Studies . . . . .	16
A.1.2 Explicit Normalization of Triggers in AIF . . . . .	23
A.1.3 Visualization of Synthesized Trojan Images and Triggers . . . . .	24
A.1.4 Qualitative Results of Our Filtering Defenses	24

## A. Appendix

### A.1. Related Work about Trojan Attacks

In this paper, we mainly consider a class of Trojan attacks in which attackers fully control the training processes of a classifier. We refer to these attacks as “full-control” attacks. There is another less common type of Trojan attacks called “clean-label” attacks [36, 40, 52]. These attacks assume a scenario in which people want to adapt a popular pretrained classifier  $C$  (e.g., ResNet [13]) for their tasks by retraining the top layers of  $C$  with additional data collected from the web. The goal of an attacker is to craft a poisoning image  $\tilde{x}$  that looks visually indistinguishable from an image  $x_t$  of the target class  $t$  while being close to some source image  $x_s$  in the feature space by optimizing the following objective:

$$\tilde{x} = \underset{x}{\operatorname{argmin}} \|C_f(x) - C_f(x_s)\|_2^2 + \lambda \|x - x_t\|_2^2$$

where  $C_f(\cdot)$  denotes the output of the penultimate layer of  $C$ . The attacker then puts  $\tilde{x}$  on the web so that it can be collected and labeled by victims. Since  $\tilde{x}$  looks like an image of the target class  $t$ ,  $\tilde{x}$  will be labeled as  $t$ . When the victims retrain  $C$  using a dataset containing  $\tilde{x}$ ,  $\tilde{x}$  will create a “backdoor” in  $C$ . The attacker can use  $x_s$  to access this “backdoor” and forces  $C$  to output  $t$ . Apart from the advantage that the attacker does not need to control the labeling process (while in fact, he can’t), the clean-label attack has several drawbacks due to its impractical assumptions. For example, the victims may retrain the whole  $C$  instead of just the last softmax layer of  $C$ ; the victims may use their own training data to which the attacker can’t access; the victims may

Dataset	#Classes	Image size	Attack		Defense	
			#Train	#Test	#Train	#Test
MNIST	10	28×28×1	60000	10000	7000	3000
CIFAR10	10	32×32×3	50000	10000	7000	3000
GTSRB	43	32×32×3	39209	12630	8826	3804
CelebA	8	64×64×3	162770	19867	13904	5963

Table 4: Datasets used in our experiments.

use  $C$  for a completely new task that the attacker does not know; the attacker doesn’t even know who are the victims. Moreover, since  $x_s$  often looks very different from images of the target class  $t$ ,  $x_s$  can be easily detected by human inspection at test time.

Compared to clean-label attacks, full-control attacks are much harder to defend against because attackers have all freedom to do whatever they want with  $C$  before sending it to the victims. BadNet [10], Blended Injection [3] are among the earliest attacks [15, 24] of this type that use only one global trigger and use image blending as an injection function. These attacks can be mitigated by well-known defenses like Neural Cleanse [47] or STRIP. Besides, their triggers also look unnatural. Therefore, subsequent attacks focus mainly on improving the robustness and stealthiness of triggers at test time. Some attacks use dynamic and/or input-specific triggers [19, 31, 32, 37]. Others use more advanced injection functions [23, 32] or GANs [30] to create hidden triggers or use physical objects as triggers [3, 49].

### A.2. Datasets

We provide details of the datasets used in our experiments in Table 4. The training and test sets for defense ( $\mathcal{D}_{\text{val}}$  and  $\mathcal{D}_{\text{test}}$ ) are taken from the test set for attack with the training/test proportion of 0.7/0.3.

### A.3. Model Architectures and Training Settings for the Attacks

**Model architectures** The classifier’s architectures in our work follow exactly those in [31, 32]. Specifically, we use PreactResNet18 [14] for CIFAR10/GTSRB, ResNet18 [13] for CelebA, and the convolutional network described in [31] for MNIST.

**Training settings** We reuse the official codes provided by the authors of Input-Aware Attack<sup>4</sup> and WaNet<sup>5</sup> for training the two attacks. We reimplement and train BadNet+, noise-BI+, image-BI+ ourselves.

Encoder	Encoder
ConvBlockX(1, 16)	ConvBlockY(3, 64)
ConvBlockX(16, 32)	ConvBlockY(64, 128)
ConvBlockX(32, 64)	ConvBlockY(128, 256)
Reshape [64, 3, 3] to [576]	ConvBlockY(256, 512)
LinearBlockX(576, 256)	
Decoder	Decoder
LinearBlockX(256, 576)	DeconvBlockY(512, 512)
Reshape [576] to [64, 3, 3]	DeconvBlockY(512, 256)
DeconvBlockX(64, 32)	DeconvBlockY(256, 128)
DeconvBlockX(32, 16)	DeconvBlockY(128, 3)
DeconvBlockX(16, 1)	
MNIST	CelebA

Table 5: Architectures of F (in AIF) for MNIST and CelebA.

LinearBlockX( $d_i, d_o$ )	
Linear( $d_i, d_o, b=False$ )	
BatchNorm2d( $d_o, m=0.01$ )	
ReLU()	
ConvBlockX( $c_i, c_o$ )	DeconvBlockX( $c_i, c_o$ )
Conv2d( $c_i, c_o, k=4, s=2, p=1, b=False$ )	ConvTranspose2d( $c_i, c_o, k=4, s=2, p=1, p_o=1, b=False$ )
BatchNorm2d( $c_o, m=0.01$ )	BatchNorm2d( $c_o, m=0.01$ )
ReLU()	ReLU()
ConvBlockY( $c_i, c_o$ )	DeconvBlockY( $c_i, c_o$ )
Conv2d( $c_i, c_o, k=4, s=2, p=1, b=False$ )	ConvTranspose2d( $c_i, c_o, k=4, s=2, p=1, b=False$ )
BatchNorm2d( $c_o, m=0.01$ )	BatchNorm2d( $c_o, m=0.01$ )
LeakyReLU(0.2)	ReLU()

Table 6: Linear, convolutional, and deconvolutional blocks of the architectures in Table 5.

#### A.4. Model Architectures, Training Settings, and Metrics for our Defenses

**Model architectures** In AIF, F is a plain autoencoder. We use the two architectures in Table 5 for F when working on MNIST and CelebA and the architecture (C) in Table 7 when working on CIFAR10/GTSRB. The remaining architectures in Table 7 are for our ablation study in Appdx. A.11.2. The architecture of G is derived from the decoder of F with additional layers to handle the noise vector  $\epsilon$ .  $\epsilon$  has a fixed length of 128. The symbols in Tables 5, 6, 7, 8 have the following meanings:  $c_i$  is input channel,  $c_o$  is output channel,  $k$  is kernel size,  $s$  is stride,  $p$  is padding,  $p_o$  is output padding,  $m$  is momentum, and  $b$  is bias.

<sup>4</sup>Input-Aware Attack: <https://github.com/VinAIRResearch/input-aware-backdoor-attack-release>  
<sup>5</sup>WaNet: [https://github.com/VinAIRResearch/Warping-based\\_Backdoor\\_Attack-release](https://github.com/VinAIRResearch/Warping-based_Backdoor_Attack-release)

The architectures of F in VIF are adapted from those of F in AIF by changing the middle layer between the encoder and decoder to produce the latent mean  $\mu_z$  and standard deviation  $\sigma_z$  that characterize  $q(z|x)$ .

**Training settings** If not otherwise specified, we train the generator G, the filter F, and the parameterized triggers  $(m_i, p_i)$  using Adam optimizer [16] (learning rate =  $1e^{-3}$ ,  $\beta_1 = 0.5, \beta_2 = 0.9$ ) for 600 epochs with batch size equal to 128. For trigger synthesis (Section 3), in Eqs. 2, the norm is L2,  $\delta = 0, \lambda_0$  varies from  $1e^{-3}$  to 1 with the multiplicative step size  $\approx 0.3$ . For VIF (Section 4.1), in Eq. 3, the norm is L2,  $\lambda_1 = 1.0$  and  $\lambda_2 = 0.003$ . An analysis of different values of  $\lambda_2$  is provided in Section 5.4.1. For AIF (Section 4.2), F and G are optimized alternately with the learning rate for G is  $3e^{-4}$ . In Eq. 7,  $\delta = 0.05, \lambda_0 = 0.01, \lambda_3 = 0.3$ . In Eq. 8,  $\lambda_1 = 0.1, \lambda_4 = 0.3, \lambda_5 = 0.01$ . To ensure that G and F are in good states before adversarial learning is conducted, we pretrain G and F for 100 epochs each. The pretraining losses for G and F are the terms  $\mathcal{L}_{\text{gen}}$  in Eq. 7 and  $\mathcal{L}_{\text{IF}}$  in Eq. 8, respectively. The training data in  $\mathcal{D}_{\text{val}}$  are augmented with random flipping, random crop (padding size = 5), and random rotation (degree = 10).

#### A.5. Results of the Attacks on $\mathcal{D}_{\text{test}}$

For completeness, we provide results of the Trojan attacks on  $\mathcal{D}_{\text{test}}$  in Table 9. These results are quite similar to the results on  $\mathcal{D}_{\text{val}} \cup \mathcal{D}_{\text{test}}$  in Table 1. We note that the decreases in clean and recovery accuracies of our defenses are computed based on the results on  $\mathcal{D}_{\text{test}}$ .

#### A.6. Full Results of the Baseline Defenses

##### A.6.1 Network Pruning

We provide the Trojan accuracies of Network Pruning (NP) [21] at 1%, 5%, and 10% decrease in clean accuracy in Table 10 and the corresponding pruning curves in Fig. 8. It is clear that NP is a very ineffective Trojan mitigation method since the classifier pruned by NP still achieves nearly 100% Trojan accuracies on CIFAR10, GTSRB, and CelebA even when experiencing about 10% decrease in clean accuracy.

##### A.6.2 STRIP

In Table 11, we report the false negative rates (FNRs) of STRIP at 1%, 5%, and 10% false positive rate (FPR). We also provide the AUCs and the entropy histograms of STRIP in Figs. 9 and 10, respectively. Note that AUCs are only suitable for experimental purpose not practical use since in real-world scenarios, we still have to compute thresholds based on FPRs on clean data. STRIP achieves very high FNRs on MNIST, CIFAR10, and GTSRB when defending against InpAwAtk and WaNet (Table 11) which corresponds to low AUCs (Fig. 9).

Encoder	Encoder	Encoder	Encoder
ConvBlockA(3, 32, $k=5$ , $s=1$ )	ConvBlockB(3, 32)	ConvBlockC(3, 32)	ConvBlockC(3, 32) $\rightarrow z_1$
ConvBlockA(32, 64, $k=4$ , $s=2$ )	ConvBlockB(32, 32)	MaxPool2d(2, 2)	MaxPool2d(2, 2)
ConvBlockA(64, 128, $k=4$ , $s=1$ )	MaxPool2d(2, 2)	ConvBlockC(32, 64)	ConvBlockC(32, 64) $\rightarrow z_2$
ConvBlockA(128, 256, $k=4$ , $s=2$ )	ConvBlockB(32, 64)	MaxPool2d(2, 2)	MaxPool2d(2, 2)
ConvBlockA(256, 512, $k=4$ , $s=1$ )	ConvBlockB(64, 64)	ConvBlockC(64, 128)	ConvBlockC(64, 128) $\rightarrow z$
ConvBlockA(512, 512, $k=1$ , $s=1$ )	MaxPool2d(2, 2)		
Linear(512, 256)	ConvBlockB(64, 128)		
	ConvBlockB(128, 128)		
	MaxPool2d(2, 2)		
	ConvBlockB(128, 128)		

Decoder	Decoder	Decoder	Decoder
DeconvBlockA(256, 256, $k=4$ , $s=1$ )	UpsamplingBilinear2d(2)	UpsamplingBilinear2d(2)	ConvTranspose2d(128, 64, $k=2$ , $s=2$ ) $\rightarrow y_2$
DeconvBlockA(256, 128, $k=4$ , $s=2$ )	ConvBlockB(128, 128)	ConvBlockC(128, 64)	Concat( $[y_2, z_2]$ )
DeconvBlockA(128, 64, $k=4$ , $s=1$ )	ConvBlockB(128, 64)	UpsamplingBilinear2d(2)	ConvBlockC(128, 64)
DeconvBlockA(64, 32, $k=4$ , $s=2$ )	UpsamplingBilinear2d(2)	ConvBlockC(64, 32)	ConvTranspose2d(64, 32, $k=2$ , $s=2$ ) $\rightarrow y_1$
DeconvBlockA(32, 32, $k=5$ , $s=1$ )	ConvBlockB(64, 64)	Conv2d(32, 3, $k=1$ )	Concat( $[y_1, z_1]$ )
DeconvBlockA(32, 32, $k=1$ , $s=1$ )	ConvBlockB(64, 32)		ConvBlockC(64, 32)
ConvTranspose2d(32, 3, $k=1$ , $s=1$ )	UpsamplingBilinear2d(2)		Conv2d(32, 3, $k=1$ )
	ConvBlockB(32, 32)		
	Conv2d(32, 3, $k=3$ , $p=1$ )		

(A)	(B)	(C)	(D)
-----	-----	-----	-----

Table 7: Architectures of F (in AIF) for CIFAR10 and GTSRB.

ConvBlockA( $c_i, c_o, k, s$ )	DeconvBlockA( $c_i, c_o, k, s$ )	ConvBlockB( $c_i, c_o$ )	ConvBlockC( $c_i, c_o$ )
Conv2d( $c_i, c_o, k, s$ )	ConvTranspose2d( $c_i, c_o, k, s$ )	Conv2d( $c_i, c_o, k=3, p=1$ )	Conv2d( $c_i, c_o, k=3, p=1$ )
BatchNorm2d( $c_o, m=0.1$ )	BatchNorm2d( $c_o, m=0.1$ )	BatchNorm2d( $c_o, m=0.05$ )	ReLU()
LeakyReLU()	LeakyReLU()	ReLU()	BatchNorm2d( $c_o, m=0.01$ )
			Conv2d( $c_o, c_o, k=3, p=1$ )
			ReLU()
			BatchNorm2d( $c_o, m=0.01$ )

Table 8: Convolutional and deconvolutional blocks of the architectures in Table 7.

### A.6.3 Neural Cleanse

After classifying C as Trojan-infected, Neural Cleanse (NC) mitigates Trojans via pruning C or checking input images. We refer to these two methods as *Neural Cleanse Pruning (NCP)* and *Neural Cleanse Input Checking (NCIC)*. Both methods build a set of synthesized Trojan images by embedding the synthesized trigger corresponding to the detected target class on all clean images in  $\mathcal{D}_{\text{val}}$ . NCP ranks neurons in the second last layer of C according to their average activation gaps computed on the synthesized Trojan images and the corresponding clean images in  $\mathcal{D}_{\text{val}}$  in descending order. It gradually prunes the neurons with the highest ranks first until certain decrease in clean accuracy is met. NCIC, on the other hand, picks the top 1% of the neurons in the second last layer of C with largest average activations on the synthesized Trojan images to form a characteristic group of Trojan neurons. Given an input image  $x$ , NCIC considers

the mean activations of the neurons in the group w.r.t.  $x$  as a score for detecting whether  $x$  contains Trojan triggers or not. If the score is greater than a threshold,  $x$  is considered as a Trojan image, otherwise, a clean image. The threshold is chosen based on the scores of all clean images in  $\mathcal{D}_{\text{val}}$ . We provide the results of NCP in Table 12, Fig. 11 and the results of NCIC in Table 13. At 5% decrease in clean accuracy, NCP reduces the Trojan accuracies of all the attacks except WaNet to almost 0% on MNIST and CIFAR10. However, NCP is ineffective against these attacks especially image-BI+ and InpAwAtk on GTSRB and CelebA. At 10% FPR, NCIC achieves nearly perfect FNRs against BadNet+, noise-BI+, and image-BI+ on all datasets but is also ineffective against InpAwAtk on GTSRB and CelebA. Note that both NCP and NCIC have almost no effect against WaNet on MNIST, CIFAR10, and CelebA since NC misclassifies the Trojan classifiers w.r.t. this attack as benign.

Dataset	Benign	BadNet+		noise-BI+		image-BI+		InpAwAtk		WaNet	
	Clean	Clean	Trojan	Clean	Trojan	Clean	Trojan	Clean	Trojan	Clean	Trojan
MNIST	99.57	99.47	99.97	99.35	100.0	99.37	100.0	99.33	99.30	99.50	99.07
CIFAR10	94.71	94.83	100.0	94.57	100.0	95.13	99.90	94.57	99.40	94.27	99.67
GTSRB	99.63	99.42	100.0	99.45	100.0	99.34	100.0	98.97	99.66	99.16	99.42
CelebA	78.82	79.57	100.0	78.32	100.0	78.82	100.0	78.17	100.0	78.18	99.97

Table 9: Clean and Trojan accuracies of *single-target* attacks on the defense test set ( $\mathcal{D}_{\text{test}}$ ) of different datasets.

Dataset	BadNet+			noise-BI+			image-BI+			InpAwAtk			WaNet		
	1%	5%	10%	1%	5%	10%	1%	5%	10%	1%	5%	10%	1%	5%	10%
MNIST	37.38	22.73	14.98	14.21	11.00	6.75	14.69	6.31	4.72	3.32	3.32	3.32	1.18	1.18	1.18
CIFAR10	100.0	100.0	100.0	99.33	87.26	87.26	99.74	99.74	99.74	56.52	56.52	56.52	96.85	96.59	96.59
GTSRB	100.0	100.0	100.0	100.0	100.0	100.0	99.87	99.87	99.87	18.38	18.38	18.38	98.86	98.86	98.86
CelebA	84.08	63.35	50.64	100.0	99.97	99.97	99.87	99.87	99.80	100.0	100.0	99.97	98.22	88.48	53.10

Table 10: Trojan accuracies of C pruned by Network Pruning at 1%, 5%, and 10% decrease in clean accuracy. *Lower values are better*. Results are computed on  $\mathcal{D}'_{\text{test}}$ .

#### A.6.4 Februus

We reimplement Februus based on the official code provided by the authors<sup>6</sup>. Since there is no script for training the inpainting GAN in the authors’ code, we use the “inpaint” function from OpenCV instead. Februus has 2 main hyperparameters that need to be tuned which are: i) the convolutional layer of C at which GradCAM computes heatmaps (“heatmap layer” for short) and ii) the threshold for converting GradCAM heatmaps into binary masks (“binary threshold” for short). As shown in Fig. 13, the performance of Februus greatly depends on these hyperparameters. Increasing the binary threshold means smaller areas are masked and inpainted, which usually leads to smaller decreases in clean accuracy (smaller  $\downarrow$ Cs) yet higher Trojan accuracies (higher Ts). Meanwhile, choosing top layers of C to compute heatmap (e.g., layer4) usually causes bigger  $\downarrow$ Cs yet lower Ts since the selected regions are often broader (Fig. 12). For simplicity, we choose the (layer, threshold) setting that gives the smallest decrease in recovery accuracy ( $\downarrow$ R) of Februus when defending against BadNet+ and apply this setting to all other attacks.

#### A.7. Full Results of Our FtC Defenses

In Table 14, we show the full results our FtC defenses (IFtC, VIFtC, AIFtC). These results are highly correlated with the results of our filtering defenses (IF, VIF, AIF) in Table 2.

#### A.8. Results of All-target Attacks

We provide the clean and Trojan accuracies of different *all-target* attacks on  $\mathcal{D}_{\text{test}}$  in Table 15. We do not consider WaNet in this experiment because we could not successfully train the all-target version of WaNet.

#### A.9. Results of Our Proposed Defenses against All-target Attacks

In Tables 16 and 17, we show the results our filtering and FtC defenses against different *all-target* attacks. On CIFAR10 and GTSRB, VIF/VIFtC and AIF/AIFtC are comparable. However, on MNIST, AIF/AIFtC is clearly better than VIF/VIFtC.

#### A.10. BadNet+ and Noise/Image-BI+

**BadNet+** *BadNet+* is a variant of BadNet [10] that uses  $M$  different image patches  $p_0, \dots, p_{M-1}$  ( $p_m \in \mathbb{I}^{c \times h_p \times w_p}$ ,  $0 \leq m < M$ ) as Trojan triggers. Each patch  $p_m$  is associated with a 2-tuple  $l_m = (i, j)$  specifying the location of this patch in an input image, where  $0 \leq i < h - h_p$  and  $0 \leq j < w - w_p$ . The pixel values and locations of the patches are generated randomly during construction. If not otherwise specified, we set  $M = 20$  and set the patch size  $h_p \times w_p$  to be  $5 \times 5$  for MNIST, CIFAR10, GTSRB, and  $8 \times 8$  for CelebA.

**Blended Injection+** *Blended Injection+* (BI+) is similar to BadNet+ except that it uses *full-size images*  $\rho_0, \dots, \rho_{M-1}$  ( $\rho_m \in \mathbb{I}^{c \times h \times w}$ ,  $0 \leq m < M$ ) as triggers instead of patches. Given a clean image  $x$  and a Trojan-triggering image  $\rho_m$ , the corresponding Trojan image  $\tilde{x}$  is computed as follows:

$$\tilde{x} = (1 - \alpha) \cdot x + \alpha \cdot \rho_m$$

where  $\alpha$  is the blending ratio set to 0.1 by default.

$\rho_0, \dots, \rho_{M-1}$  can be either random noises or real images, resulting in two sub-versions of BI+, namely *noise-BI+* and *image-BI+*. Choosing good Trojan-triggering images for image-BI+ is non-trivial. We tried various real images

<sup>6</sup><https://github.com/AdelaideAuto-IDLab/Februus>

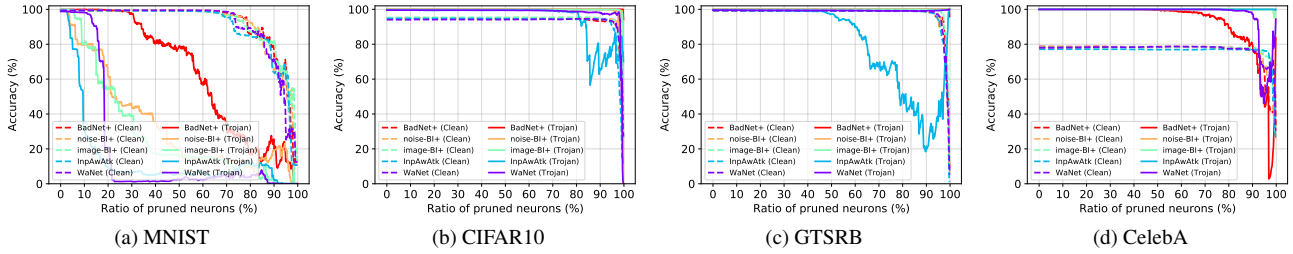


Figure 8: Clean accuracy (dashed) and Trojan accuracy (solid) curves of  $C$  pruned by Network Pruning for different attacks and datasets which correspond to the results in Table 10.

Dataset	BadNet+			noise-BI+			image-BI+			InpAwAtk			WaNet		
	1%	5%	10%	1%	5%	10%	1%	5%	10%	1%	5%	10%	1%	5%	10%
MNIST	88.45	64.40	36.25	13.95	0.00	0.00	16.40	0.05	0.00	99.95	99.80	99.15	99.85	97.55	92.40
CIFAR10	0.00	0.00	0.00	10.35	2.35	0.95	99.45	97.30	95.75	99.55	97.90	96.20	100.0	99.25	96.90
GTSRB	1.05	0.20	0.00	0.00	0.00	0.00	79.20	58.30	44.75	99.85	98.80	97.15	99.50	96.00	91.65
CelebA	17.50	11.20	7.70	33.80	19.80	14.70	75.75	62.35	54.45	1.90	1.20	1.00	99.80	98.55	96.20

Table 11: False negative rates (FNRs) of STRIP at 1%, 5%, and 10% false positive rate (FPR) for different attacks and datasets. Lower values are better.

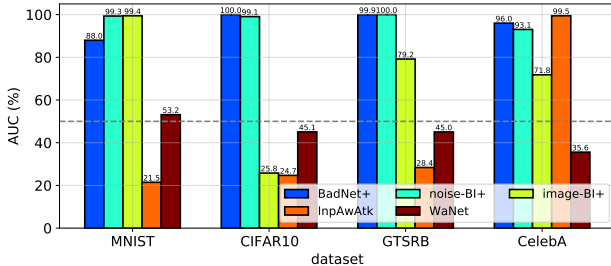


Figure 9: AUCs of STRIP against different attacks on different datasets. Higher values are better.

(Fig. 14) and found that they lead to very different attack success rates (aka *Trojan accuracies*) (Fig. 15). The best ones often contain colorful, repetitive patterns (e.g., “candies” or “crayons” images). Besides, we also observed that training image-BI+ with  $M \geq 10$  is difficult since the classifier usually needs a lot of time to remember real images. Therefore, we selected only 5 images with the highest training Trojan accuracies (images 11-15 in Fig. 14) to be used as triggers for image-BI+ in our experiments.

noise-BI+, by contrast, achieves almost perfect Trojan accuracies even when  $M$  is big ( $M \approx 100$ ). We think the main reason behind this phenomenon is that a random noise image usually have much more distinct patterns than a real image. Although blending with clean input images may destroy some patterns in the noise image, many other patterns are still unaffected and can successfully cause the classifier to output the target class.

## A.11. Additional Ablation Studies

### A.11.1 Comparison between Input Filtering and Input Processing [24]

In Fig. 18, we compare the performances of our Input Filtering (IF) and Input Processing (IP) against all the attacks on all the datasets. It is clear that IF outperforms IP in terms of Trojan accuracy in most cases, especially under InputAwAtk and WaNet. For example, IP achieves very high (poor) Trojan accuracies of 34.85%, 62.33%, and 76.49% against WaNet on CIFAR10, GTSRB, and CelebA, respectively while our IF achieves only 4.82%, 9.83%, and 15.21%. These results empirically verify the importance of the term  $-\log p_C(y|x^\circ)$  in the loss of IF. This term ensures that the filtered output  $x^\circ$  computed by  $F$  cannot cause harm to  $C$  even when it look very similar to the original input  $x$ .

### A.11.2 Different architectures of the filter $F$

A major factor that affects the performance of  $F$  is its architecture. We consider an architecture of  $F$  to be more complex than others if  $F$  achieves smaller reconstruction loss on  $\mathcal{D}_{val}$  with this architecture. In Section 4, we argued that an optimal filter should be neither too simple nor too complex. Here, we empirically verify this intuition by examining 4 different architectures of  $F$  for CIFAR10 marked as A, B, C, D (Table 7). Their complexities are greater in alphabetical order as shown in Figs. 16, 17. The architecture D has skip-connections between its encoder and decoder while A, B, C do not.

Denote  $F$  with the architectures A, B, C, D as  $F_A, F_B, F_C, F_D$  respectively. As shown in Table 19,  $F_C$  is the best in terms



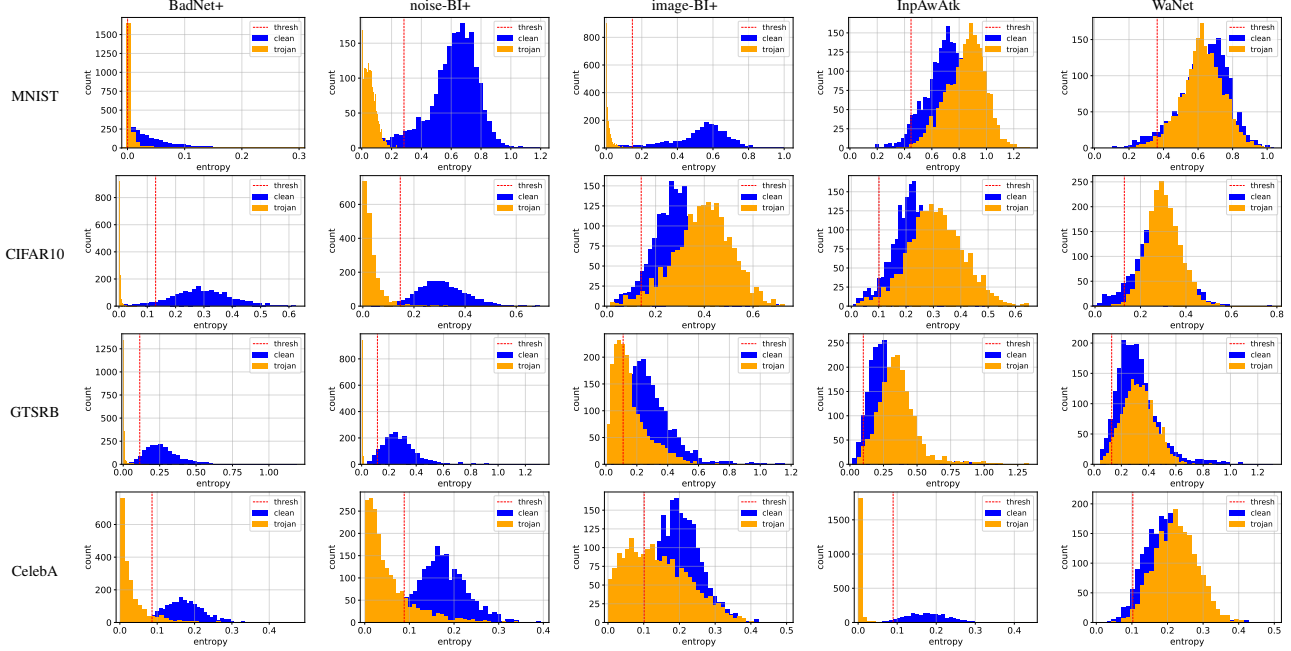


Figure 10: Histograms of entropies computed by STRIP for different attacks and datasets. The vertical red dashed line in each plot indicates the threshold at 5% false positive rate.

Dataset	BadNet+			noise-BI+			image-BI+			InpAwAtk			WaNet		
	1%	5%	10%	1%	5%	10%	1%	5%	10%	1%	5%	10%	1%	5%	10%
MNIST	0.00	0.00	0.00	0.00	0.00	0.00	0.00	0.00	0.00	0.00	0.00	0.00	-	-	-
CIFAR10	0.00	0.00	0.00	7.37	1.11	0.70	0.00	0.00	0.00	-	-	-	-	-	-
GTSRB	61.94	48.23	48.23	78.71	1.03	1.03	51.74	51.74	51.74	49.02	38.33	38.33	2.75	1.58	1.58
CelebA	75.97	26.73	7.63	99.95	98.75	95.30	99.75	96.21	83.62	99.87	98.42	93.31	-	-	-

Table 12: Trojan accuracies of the Trojan classifier C pruned by Neural Cleanse Pruning at 1%, 5%, and 10% decrease in clean accuracy for different attacks and datasets. *Lower values are better.* Some results for InpAwAtk and WaNet are not available because Neural Cleanse fails to classify C as Trojan-infected in these cases (Fig. 4a).

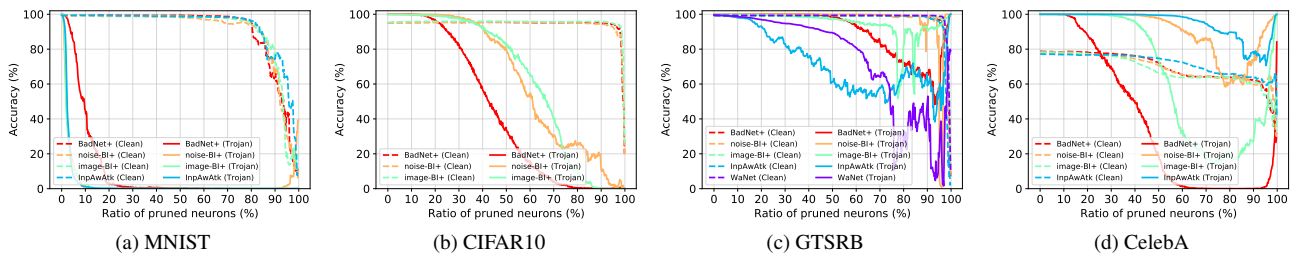


Figure 11: Clean accuracy (dashed) and Trojan accuracy (solid) curves of the Trojan classifier C pruned by Neural Cleanse Pruning for different attacks and datasets which correspond to the results in Table 12.

Dataset	BadNet+			noise-BI+			image-BI+			InpAwAtk			WaNet		
	1%	5%	10%	1%	5%	10%	1%	5%	10%	1%	5%	10%	1%	5%	10%
MNIST	9.75	4.75	3.25	0.00	0.00	0.00	0.00	0.00	0.00	0.80	0.30	0.15	-	-	-
CIFAR10	99.50	78.90	0.65	90.55	39.30	0.05	95.50	56.90	0.40	-	-	-	-	-	-
GTSRB	100.0	0.40	0.00	0.00	0.00	0.00	0.03	0.00	0.00	99.48	92.17	86.65	3.02	0.40	0.32
CelebA	2.25	0.00	0.00	17.70	0.65	0.00	50.20	11.60	2.35	88.25	42.15	13.60	-	-	-

Table 13: False negative rates (FNRs) computed by Neural Cleanse Input Checking at 1%, 5%, and 10% false positive rate (FPR) for different attacks and datasets. *Lower values are better.*

Dataset	Defense	Benign	BadNet+		noise-BI+		image-BI+		InpAwAtk		WaNet	
		FPR	FPR	FNR	FPR	FNR	FPR	FNR	FPR	FNR	FPR	FNR
MNIST	IFtC	0.40	0.50	<b>2.21</b>	0.37	0.22	0.37	1.51	0.53	<b>1.71</b>	0.60	1.33
	VIFtC	0.27	<b>0.30</b>	2.84	0.23	<b>0.07</b>	0.40	0.15	0.47	1.99	0.30	1.51
	AIFtC	<b>0.23</b>	0.32	4.17	<b>0.17</b>	0.15	<b>0.17</b>	<b>0.11</b>	<b>0.33</b>	1.87	<b>0.13</b>	<b>1.18</b>
CIFAR10	IFtC	<b>6.83</b>	<b>7.47</b>	<b>1.70</b>	<b>6.57</b>	0.93	<b>7.83</b>	36.56	<b>7.25</b>	16.89	<b>7.17</b>	5.15
	VIFtC	12.30	11.00	2.63	10.67	1.26	11.03	10.89	10.63	<b>3.67</b>	11.40	4.26
	AIFtC	8.63	8.87	1.96	8.73	<b>0.89</b>	8.77	<b>2.15</b>	8.27	5.93	7.93	<b>1.56</b>
GTSRB	IFtC	<b>0.38</b>	0.45	<b>0.00</b>	0.24	0.03	0.66	52.91	<b>0.29</b>	1.00	0.66	10.41
	VIFtC	0.45	0.74	0.03	0.47	<b>0.00</b>	0.87	12.63	0.53	<b>0.37</b>	1.31	4.25
	AIFtC	0.50	<b>0.37</b>	0.03	0.39	<b>0.00</b>	<b>0.63</b>	<b>7.87</b>	0.47	0.40	<b>0.60</b>	<b>1.08</b>
CelebA	IFtC	<b>14.24</b>	<b>15.78</b>	8.36	<b>14.94</b>	14.25	<b>13.99</b>	59.43	<b>12.84</b>	11.95	<b>13.08</b>	15.27
	VIFtC	17.74	18.90	9.09	18.50	<b>11.67</b>	18.09	<b>14.30</b>	16.37	11.54	17.22	<b>8.34</b>
	AIFtC	20.24	20.95	<b>7.71</b>	19.08	12.82	19.29	18.65	16.54	<b>10.43</b>	16.55	12.87

Table 14: False positive rates (FPRs) and false negative rates (FNRs) of our FtC defenses (IFtC, VIFtC, AIFtC) against different Trojan attacks on different datasets. *Lower values are better.* For a particular attack, dataset, and metric, the best defense is highlighted in bold.

Dataset	BadNet+		noise-BI+		image-BI+		InpAwAtk	
	Clean	Trojan	Clean	Trojan	Clean	Trojan	Clean	Trojan
MNIST	99.37	98.54	99.57	99.38	99.53	99.25	99.23	97.64
CIFAR10	94.63	94.30	94.32	93.77	94.70	94.06	94.53	94.10
GTSRB	99.63	99.08	99.58	99.06	99.37	99.08	99.16	99.29

Table 15: Test clean and Trojan accuracies of different *all-target* attacks on  $\mathcal{D}_{\text{test}}$ .

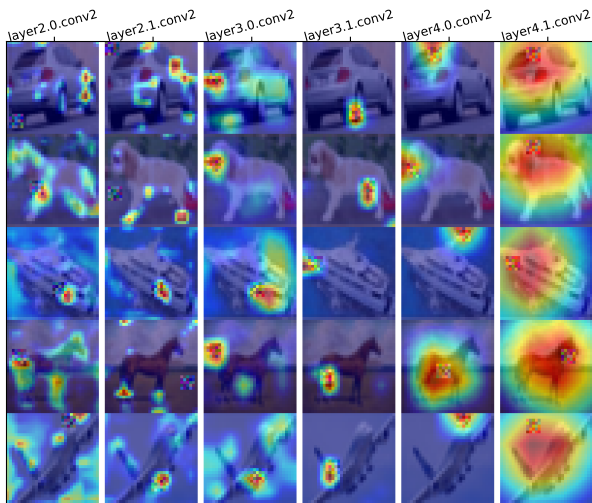


Figure 12: Examples of heatmaps computed by Februous’s GradCAM at different layers of C ordered from bottom (layer2.0.conv2) to top (layer4.1.conv2). The dataset is CIFAR10 and the classifier is a PreActResNet18 [14]. The Trojan attack is BadNet+. It is clear that only some layers give reasonably good results.

of recovery accuracy although C is neither the simplest (A) nor the most complex architecture (D).  $F_A$  achieves reasonably low Trojan accuracies comparable to those of  $F_B$  and  $F_C$  but the worst clean accuracies.  $F_D$ , by contrast, experiences almost no decrease in clean accuracy but achieves very high Trojan accuracies. The reason is that  $F_D$  simply copies all information from an input to the output via its skip-connections rather than learning compressed latent representations of input images. One can verify this by observing that the  $D_{\text{KL}}$  (Eq. 3) of  $F_D$  is almost 0 (Fig. 18c). In this case, changing  $\lambda_2$  has no effect on the Trojan accuracy of  $F_D$  as shown in Fig. 19. However, it is still possible to lower the Trojan accuracy of  $F_D$  without removing the skip-connections in D. For example, we can treat the latent representations corresponding to the skip-connections as random variables and apply the  $D_{\text{KL}}$  to these variables like what we do with the middle representation. Or we can compress the whole  $F_D$  by using advanced network compression techniques [29, 26, 45]. These ideas are out of scope of this paper so we leave them for future work.

### A.11.3 Different amount of training data

We are curious to know how well our proposed defenses will perform if we reduce the amount of training data. We select the proportion of training data from {0.8, 0.6, 0.4, 0.2, 0.1,

Dataset	Defense	BadNet+			noise-BI+			image-BI+			InpAwAtk		
		↓C	T	↓R	↓C	T	↓R	↓C	T	↓R	↓C	T	↓R
MNIST	IF	0.00	75.90	76.30	-0.03	99.30	99.47	0.13	6.96	6.96	0.00	95.74	96.17
	VIF	<b>-0.07</b>	49.67	50.17	<b>-0.07</b>	4.06	4.23	0.07	0.20	0.23	<b>-0.23</b>	63.58	64.21
	AIF	0.47	19.31	<b>20.27</b>	0.13	<b>0.03</b>	<b>0.10</b>	<b>0.03</b>	<b>0.03</b>	<b>0.13</b>	-0.13	<b>23.90</b>	<b>24.53</b>
CIFAR10	IF	<b>3.93</b>	1.57	<b>8.03</b>	<b>2.63</b>	1.17	<b>3.30</b>	<b>3.60</b>	18.90	22.20	<b>3.83</b>	9.97	14.63
	VIF	8.13	1.87	12.73	6.27	1.33	6.72	6.83	5.67	11.90	7.96	<b>5.95</b>	16.87
	AIF	5.67	<b>1.23</b>	9.13	4.40	<b>0.97</b>	5.47	5.13	<b>5.10</b>	<b>9.63</b>	5.43	6.73	<b>14.33</b>
GTSRB	IF	0.29	<b>0.11</b>	<b>1.58</b>	0.13	<b>0.21</b>	<b>1.18</b>	<b>-0.26</b>	61.57	62.25	0.11	3.97	4.50
	VIF	0.47	0.32	3.36	0.32	0.37	1.26	0.16	6.28	8.23	0.11	<b>0.60</b>	<b>1.58</b>
	AIF	<b>0.11</b>	0.29	2.08	<b>-0.05</b>	0.29	1.74	0.11	<b>1.21</b>	<b>3.23</b>	<b>-0.16</b>	2.02	2.39

Table 16: Decreases in clean accuracy (↓Cs), Trojan accuracies (Ts), and recovery accuracies (↓Rs) of our filtering defenses (IF, VIF, AIF) against different *all-target* Trojan attacks on different datasets. *Lower values are better*. For a particular dataset, attack, and metric, the best defense is highlighted in bold.

Dataset	Defense	BadNet+		noise-BI+		image-BI+		InpAwAtk	
		FPR	FNR	FPR	FNR	FPR	FNR	FPR	FNR
MNIST	IFtC	<b>0.20</b>	77.83	0.10	99.63	0.23	7.22	<b>0.20</b>	97.44
	VIFtC	<b>0.20</b>	49.97	<b>0.07</b>	4.19	<b>0.07</b>	0.27	0.33	64.85
	AIFtC	0.70	<b>19.24</b>	0.27	<b>0.07</b>	0.30	<b>0.07</b>	0.40	<b>24.83</b>
CIFAR10	IFtC	<b>7.13</b>	1.00	<b>6.10</b>	<b>0.70</b>	<b>6.70</b>	18.57	<b>6.30</b>	9.97
	VIFtC	12.10	1.30	10.14	1.12	10.50	<b>5.40</b>	11.13	<b>5.83</b>
	AIFtC	9.07	<b>0.87</b>	8.03	1.10	8.47	<b>5.40</b>	8.90	6.70
GTSRB	IFtC	0.50	<b>0.08</b>	0.29	0.29	<b>0.42</b>	62.57	<b>0.34</b>	3.97
	VIFtC	0.68	0.32	0.58	0.47	0.84	6.15	0.58	<b>0.55</b>
	AIFtC	<b>0.34</b>	0.42	<b>0.26</b>	<b>0.26</b>	0.79	<b>0.92</b>	0.45	2.05

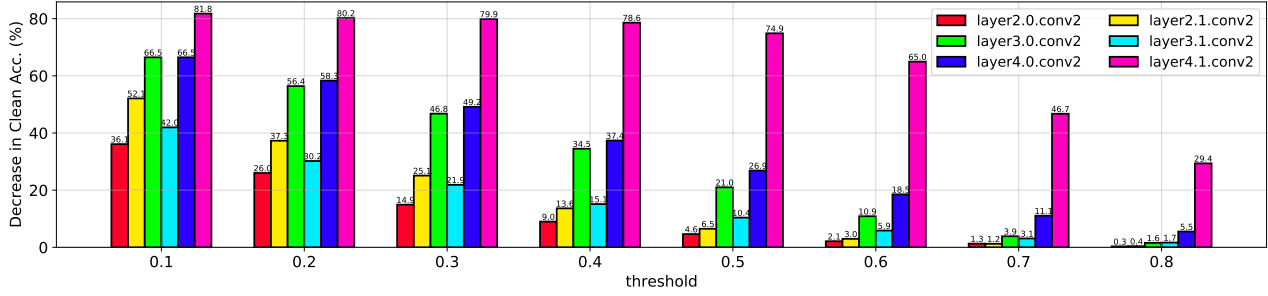
Table 17: False positive rates (FPRs) and false negative rates (FNRs) of our FtC defenses (IFtC, VIFtC, AIFtC) against different *all-target* Trojan attacks on different datasets. *Lower values are better*. For a particular dataset, attack, and metric, the best defense is highlighted in bold.

Dataset	Def.	BadNet+			noise-BI+			image-BI+			InpAwAtk			WaNet		
		↓C	T	↓R	↓C	T	↓R	↓C	T	↓R	↓C	T	↓R	↓C	T	↓R
MNIST	IP	0.37	<b>1.29</b>	<b>3.60</b>	<b>0.03</b>	3.69	<b>10.92</b>	<b>0.13</b>	1.81	<b>11.72</b>	0.30	1.14	2.10	<b>0.20</b>	1.66	1.70
	IF	<i>0.27</i>	<i>2.47</i>	<i>4.99</i>	<i>0.10</i>	<i>0.16</i>	<i>13.52</i>	<i>0.13</i>	<i>1.29</i>	<i>12.02</i>	<i>0.21</i>	<i>0.96</i>	<i>2.08</i>	<i>0.23</i>	<i>0.34</i>	<i>0.61</i>
CIFAR10	IP	4.23	2.74	8.60	3.60	<b>0.78</b>	4.97	<b>4.27</b>	<b>35.85</b>	<b>33.60</b>	5.20	20.48	22.80	5.37	34.85	30.37
	IF	<b>4.15</b>	<b>2.30</b>	<b>7.79</b>	<b>3.32</b>	<i>1.01</i>	<b>4.43</b>	<i>4.76</i>	<i>37.48</i>	<i>34.30</i>	<b>4.47</b>	<b>16.35</b>	<b>18.96</b>	<b>3.21</b>	<b>4.82</b>	<b>6.80</b>
GTSRB	IP	0.18	<b>0.00</b>	2.79	0.24	<b>0.00</b>	1.76	<b>0.37</b>	52.61	52.37	0.42	2.06	3.76	10.73	62.33	61.33
	IF	<b>0.13</b>	<b>0.00</b>	<b>2.55</b>	<b>0.13</b>	<i>0.03</i>	<b>1.52</b>	<b>0.37</b>	<b>52.27</b>	<b>51.95</b>	<b>0.03</b>	<b>0.66</b>	<b>3.60</b>	<b>0.08</b>	<b>9.83</b>	<b>9.62</b>
CelebA	IP	<b>2.83</b>	9.98	4.23	2.73	25.57	14.72	2.43	73.63	35.82	<b>2.31</b>	15.09	7.81	<b>2.28</b>	76.49	36.76
	IF	<i>4.21</i>	<b>8.62</b>	<b>4.75</b>	<i>2.57</i>	<b>13.83</b>	<b>6.00</b>	<i>2.25</i>	<b>59.39</b>	<b>27.94</b>	<i>2.86</i>	<b>11.95</b>	<b>6.07</b>	<i>2.43</i>	<b>15.21</b>	<b>4.75</b>

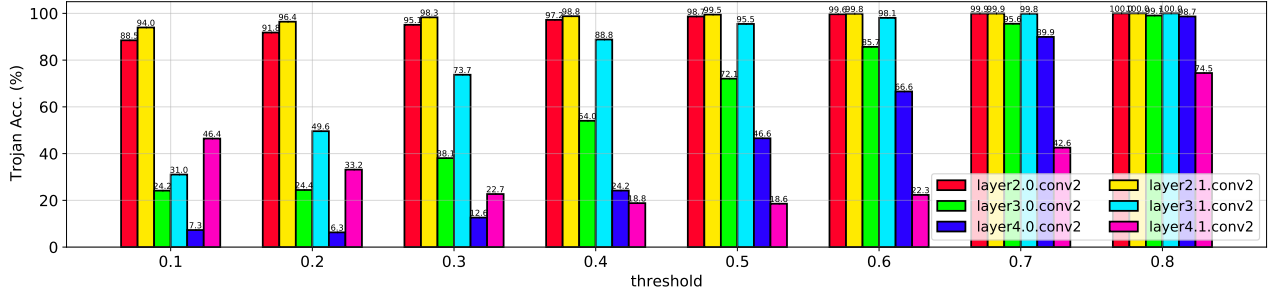
Table 18: Trojan filtering results (in %) of Input Processing [24] and our Input Filtering. For a particular dataset, attack, and metric, the best among the 2 defenses are highlighted in bold. Results taken from Table 2 are shown in italic.

Arch.	BadNet+			noise-BI+			image-BI+			InpAwAtk			WaNet		
	↓C	T	↓R	↓C	T	↓R	↓C	T	↓R	↓C	T	↓R	↓C	T	↓R
A	40.02	5.96	41.10	40.90	14.52	42.43	35.73	<b>3.56</b>	37.92	38.13	3.52	38.97	32.65	6.81	32.94
B	9.23	2.74	13.37	8.73	1.96	10.32	10.48	10.59	18.87	9.75	<b>1.96</b>	13.91	9.94	4.22	11.73
C	7.70	<b>2.52</b>	<b>11.27</b>	6.43	<b>1.22</b>	<b>7.10</b>	7.53	10.52	<b>16.50</b>	7.67	3.07	<b>12.38</b>	7.97	<b>3.96</b>	<b>10.67</b>
D	<b>0.27</b>	100.0	84.83	<b>-0.02</b>	100.0	84.57	<b>0.21</b>	99.81	84.96	<b>-0.10</b>	98.85	83.33	<b>-0.07</b>	98.96	83.35

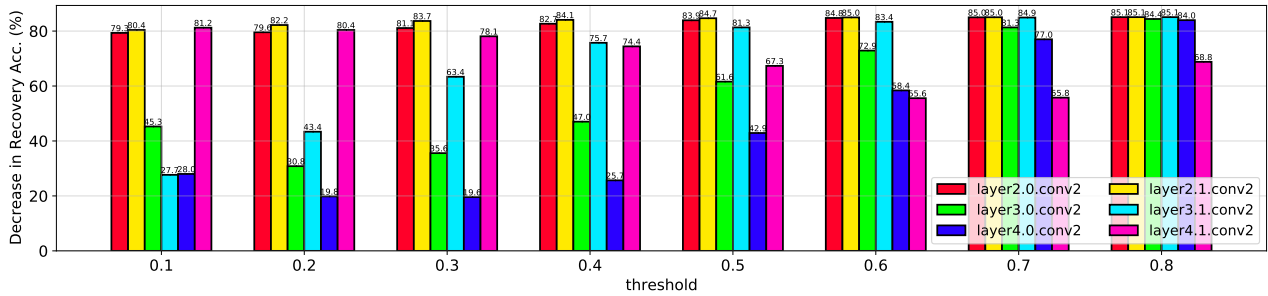
Table 19: Trojan filtering results (in %) of VIF against different attacks on CIFAR10 w.r.t. different architectures of F. For a particular dataset, attack, and metric, the best defense is highlighted in bold.



(a) Decrease in clean accuracy ( $\downarrow$ C)



(b) Trojan accuracy (T)



(c) Decrease in recovery accuracy ( $\downarrow$ R)

Figure 13: Decreases in clean accuracy (a), Trojan accuracies (b), and decreases in recovery accuracy (c) of Februs when mitigating BadNet+’s Trojans on CIFAR10 w.r.t. different heatmap layers and binary thresholds.



Figure 14: A list of Trojan-triggering images that we tried. The images are sorted by their training Trojan accuracy in ascending order. The last 5 images (11-15) were selected to be triggers for image-BI+ in our experiments.

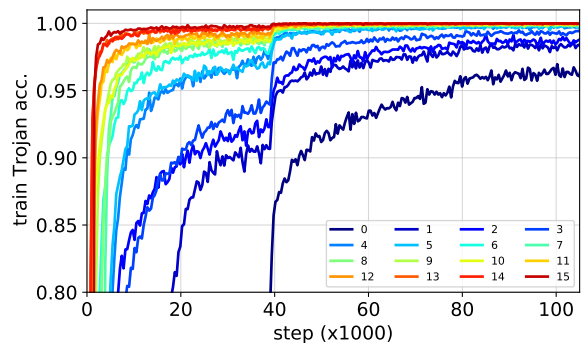


Figure 15: Training Trojan accuracy curves of BI on CIFAR10 w.r.t. different triggers in Fig. 14

0.05}. In addition, we consider two broader training settings. In the first setting, the number of training epochs is fixed at 600 (Section A.4) regardless of the amount of training

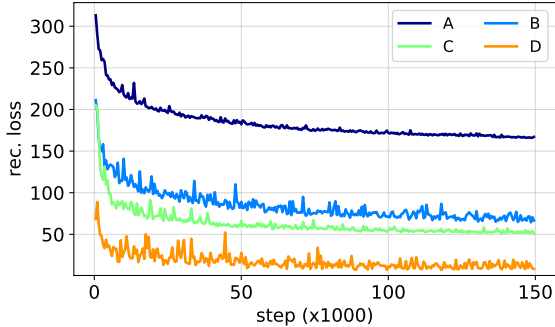


Figure 16: Reconstruction losses of the 4 autoencoders in Table 7 on CIFAR10.

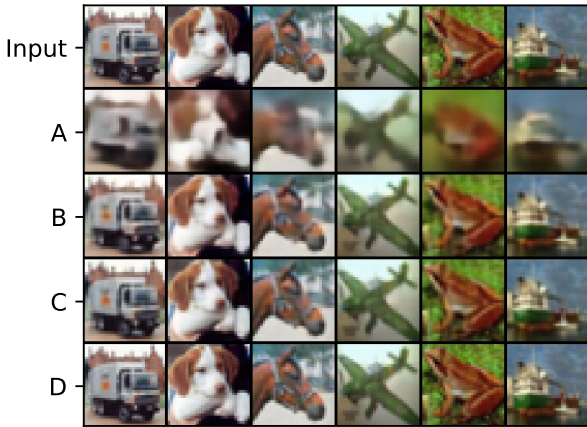


Figure 17: CIFAR10 images (top) and reconstructed images computed by the 4 autoencoders in Table 7.

data. Because less training data results in fewer iterations per epoch, fixing the number of training epochs means *smaller total number of training iterations for less training data*. In the second setting, we adjust the number of training epochs based on the proportion of training data so that the total number of training iterations is fixed and similar to that when full data is used. Table 20 shows the results of our filtering defenses w.r.t. the above settings. When the number of epochs is fixed, we see that our defenses often achieve lower Ts yet larger  $\downarrow$ Cs (and  $\downarrow$ Rs) for less training data. This is because the filter F has not been fully trained to reconstruct input images well enough (the first column in Fig. 20). On the other hand, when the total number of iterations is fixed, F has been fully trained and we do not see much difference in Trojan accuracy of VIF for different amount of training data. The Trojan accuracies of AIF slightly increase for less training data but are still acceptable (the last column in Fig. 20). Changes in clean accuracy of our defenses are small (the third column in Fig. 20). In summary, these results suggest that our proposed filtering defenses are quite robust to the limited amount of training data.

#### A.11.4 Different trigger norms

In this section, we examine the performances of our defenses against attacks using large-norm triggers. We consider BadNet+ and noise-BI+ for this study. For BadNet+, we increase the trigger norm by increasing the trigger size  $s$ . The results for BadNet+ are shown in Table 21. For noise-BI+, we increase the trigger norm by increasing the blending ratio  $\alpha$ . The results for noise-BI+ are shown in Table 22. It is clear that even when triggers have large norms, our filtering defenses, especially VIF, still effectively erase most of the trigger pixels that could activate the Trojans in C and achieve low Trojan accuracies. However, large-norm triggers cause a lot of difficulty in reconstructing the original clean images from Trojan images (Fig. 28), which leads to large decreases in recovery accuracy of our methods. Note that such poor performance is inevitable for input purification defenses like ours. A solution to this problem is using other types of defenses. For example, our FtC defenses, especially VIFtC, can be good alternatives. VIFtC achieves very low FNRs ( $<7\%$  in case of BadNet+ and  $<2\%$  in case of noise-BI+) and FPRs in an acceptable range between 10% and 15%. STRIP and Neural Cleanse are also possible (though not very good) options. STRIP works well against BadNet+ with large trigger sizes but poorly against noise-BI+ with large blending ratios (Fig. 21 left). We guess the reason is that with large blending ratios, Trojan images of noise-BI+ will look like noises and superimposing a noise-like Trojan image with a clean image is like adding noise to the clean image, hence, won't affect of the class prediction of the clean image. On the other hand, Neural Cleanse (NC) tends to wrongly identify Trojan models as benign if the behind attacks use triggers with large enough norms (Fig. 21 right). This is because the synthesized trigger w.r.t. the true target class also has large norm which is not very different from the norms of the synthesized triggers w.r.t. other classes.

#### A.11.5 VIF with/without explicit trigger normalization

From Table 23, we see that AIF with explicit trigger normalization (denoted as AIF-w) always achieve smaller  $\downarrow$ Cs and sometimes achieve larger Ts than the counterpart *without* explicit trigger normalization (denoted as AIF-wo). In general, AIF-w usually achieves lower  $\downarrow$ Rs than AIF-wo and is considered to be better so we set it as default. Fig. 22 provides a deeper insight into the results in Table 23. Without explicit trigger normalization, the generator G can easily fool F (low crossentropy losses in Fig. 22i) by just increasing the norm of the synthesized triggers (Fig. 22k). This makes  $\tilde{x}$  more different from  $x$  and causes more difficulty for F to force  $\tilde{x}^\circ$  close to  $x$  (Fig. 22h) as well as correcting the label of  $\tilde{x}$  (Fig. 22g). The large difference between  $\tilde{x}$  and  $x$  also negatively affects the performance of F on reconstructing clean images (Fig. 22f). As a result, AIF-wo achieves much

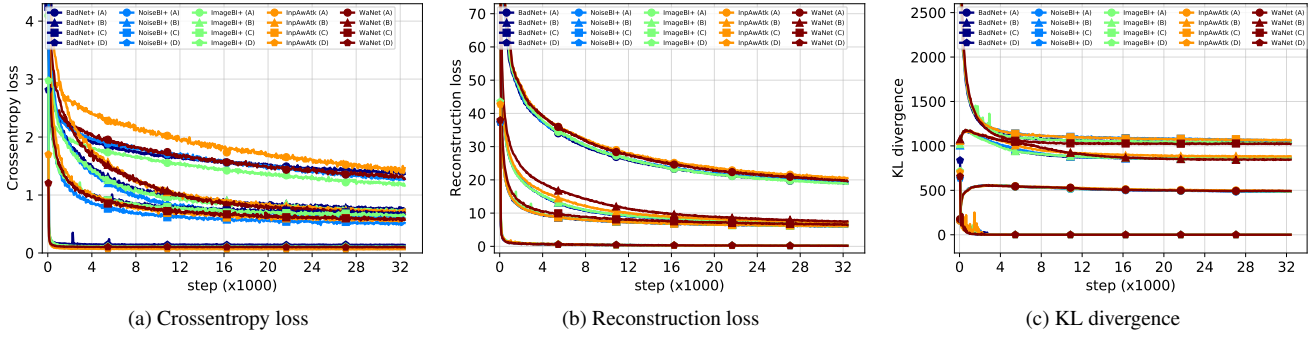


Figure 18: Training curves of VIF against InpAwAtk on CIFAR10 ( $\mathcal{D}_{\text{val}}$ ) w.r.t. the 4 architectures of F in Table 7.

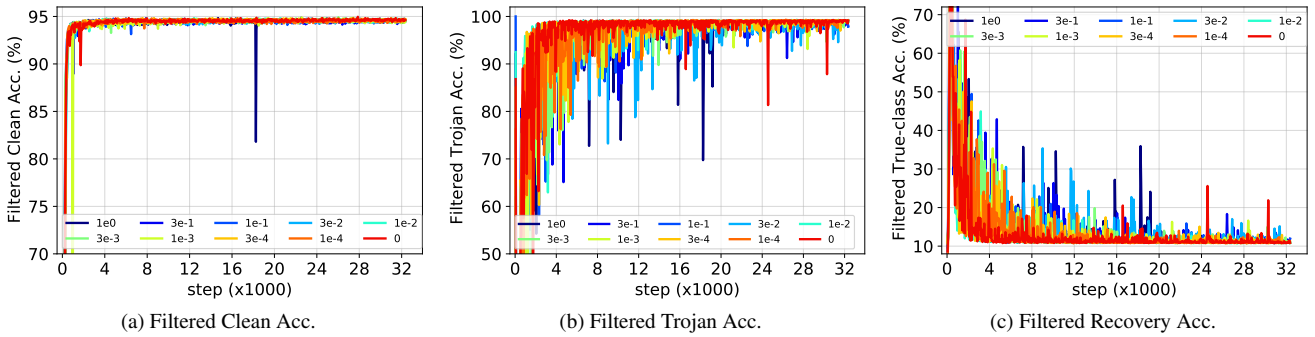


Figure 19: Test results of VIF using the architecture D (Table 7) for F against InpAwAtk on CIFAR10 ( $\mathcal{D}_{\text{test}}$ ) w.r.t. different coefficient values for  $D_{\text{KL}}$  ( $\lambda_2$  in Eq. 3).

Def.	Metric	InpAwAtk													
		Default		Fixed #epochs						Fixed total #iterations					
		1.0	0.8	0.6	0.4	0.2	0.1	0.05	0.8	0.6	0.4	0.2	0.1	0.05	
IF	↓C	<i>4.47</i>	4.73	4.43	5.37	7.90	11.60	25.93	3.53	3.87	3.83	4.20	4.23	4.87	
	T	<i>16.35</i>	15.11	11.56	9.48	6.70	4.07	6.70	16.11	15.41	20.22	18.37	26.33	21.00	
	↓R	<i>18.96</i>	19.00	15.10	15.47	15.07	17.47	32.23	18.47	18.03	21.87	20.57	26.63	23.17	
VIF	↓C	7.67	9.17	8.57	9.83	12.13	17.10	27.80	8.53	7.93	7.87	8.97	9.37	11.27	
	T	<i>3.07</i>	3.81	2.81	4.30	3.30	2.70	5.67	3.26	4.19	4.26	3.70	3.44	4.67	
	↓R	<i>12.38</i>	14.90	13.17	16.30	17.37	22.10	32.30	13.73	13.87	13.67	14.73	15.03	17.87	
AIF	↓C	5.28	5.47	6.53	7.90	11.70	16.67	26.13	5.07	5.23	5.17	6.17	5.77	7.83	
	T	<i>5.30</i>	4.96	3.59	4.89	3.15	2.89	4.00	6.63	9.04	5.70	4.56	8.48	12.96	
	↓R	<i>11.87</i>	11.60	11.90	13.87	17.03	21.80	30.40	11.73	13.83	11.77	12.57	14.50	19.93	

Table 20: Trojan filtering results (in %) of IF, VIF, and AIF against InpAwAtk on CIFAR10 w.r.t. different proportions of training data (the third row) and two broader training settings (the second row): i) fixed number of epochs, and ii) fixed total number of iterations. Results taken from Table 2 are shown in italic.

Defense	BadNet+																			
	$s = 5$					$s = 11$					$s = 17$					$s = 23$				
	↓C	T	↓R	FPR	FNR	↓C	T	↓R	FPR	FNR	↓C	T	↓R	FPR	FNR	↓C	T	↓R	FPR	FNR
IF/IFc	<i>4.15</i>	2.30	<i>7.79</i>	<i>7.47</i>	<i>1.70</i>	5.83	6.33	29.27	<b>8.83</b>	6.81	<b>4.17</b>	22.52	52.50	<b>6.83</b>	22.37	<b>4.30</b>	64.41	78.77	<b>7.47</b>	63.74
VIF/VIFc	7.70	2.52	<i>11.27</i>	<i>11.00</i>	<i>2.63</i>	11.07	3.89	31.07	14.43	3.85	9.13	<b>5.41</b>	55.60	12.80	<b>4.89</b>	9.77	<b>7.22</b>	77.73	14.07	<b>6.81</b>
AIF/AIFc	5.60	2.37	<i>9.03</i>	<i>8.87</i>	<i>1.96</i>	<b>5.53</b>	<b>3.33</b>	<b>23.97</b>	9.03	<b>3.15</b>	4.67	7.56	<b>48.40</b>	8.30	8.04	5.10	28.07	<b>77.70</b>	8.30	28.0
AIF*/AIFc*	5.90	<b>2.15</b>	10.00	9.30	2.15	6.50	5.00	34.33	9.97	5.30	5.77	14.63	52.67	9.33	13.70	6.97	29.96	77.93	10.60	30.19

Table 21: Trojan filtering results (in %) of IF, VIF, AIF, and AIF without explicit trigger normalization (AIF\*) against BadNet+ with different trigger sizes ( $s$ ) on CIFAR10. For a particular trigger size and metric, the best result is highlighted in bold. Results taken from Tables 2, 14 are shown in italic.

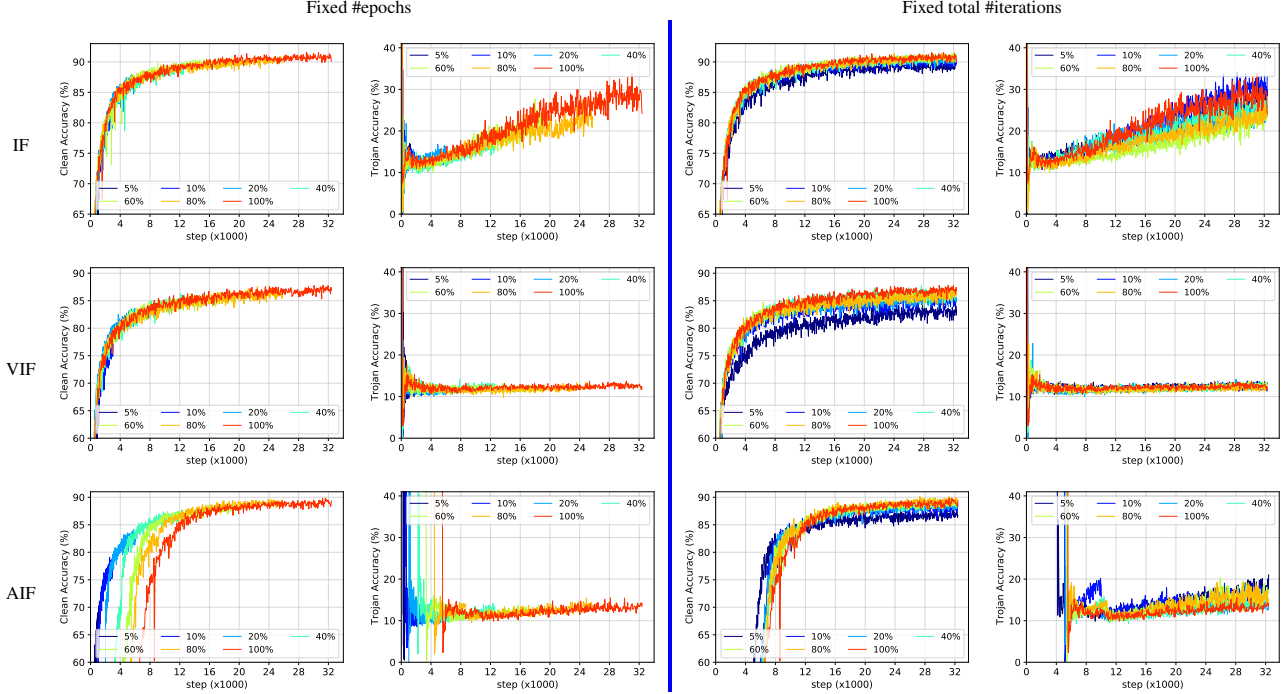


Figure 20: Test clean accuracy and Trojan accuracy curves of our filtering defenses (IF, VIF, AIF) against InpAwAtk on CIFAR10 w.r.t. different proportions of training data and 2 broader training settings: i) fixed number of epochs and ii) fixed total number of iterations.

Defense	noise-BI+																			
	$\alpha = 0.1$					$\alpha = 0.3$					$\alpha = 0.5$					$\alpha = 0.7$				
	$\downarrow C$	T	$\downarrow R$	FNR	FPR	$\downarrow C$	T	$\downarrow R$	FNR	FPR	$\downarrow C$	T	$\downarrow R$	FNR	FPR	$\downarrow C$	T	$\downarrow R$	FNR	FPR
IF/IFC	<b>3.32</b>	<i>1.01</i>	<b>4.43</b>	<b>6.57</b>	<i>0.93</i>	<b>4.30</b>	1.26	36.73	<b>7.80</b>	1.19	<b>3.53</b>	27.59	73.03	<b>7.10</b>	26.74	<b>3.87</b>	49.37	83.10	<b>7.13</b>	49.00
VIF/VIFC	<i>6.43</i>	<i>1.22</i>	<i>7.10</i>	<i>10.67</i>	<i>1.26</i>	7.53	1.44	27.57	11.80	1.56	7.67	<b>0.74</b>	<b>67.33</b>	11.63	<b>0.74</b>	7.93	<b>0.22</b>	80.80	11.57	<b>0.26</b>
AIF/AIFC	<i>4.87</i>	<i>1.14</i>	<i>6.02</i>	<i>8.73</i>	<i>0.89</i>	4.90	1.33	39.50	8.60	1.37	5.30	7.00	72.30	9.10	7.11	6.07	31.41	<b>80.70</b>	8.87	31.67
AIF*/AIFC*	5.60	<b>0.78</b>	7.50	9.53	<b>0.74</b>	6.07	<b>0.48</b>	45.13	10.10	<b>0.74</b>	6.27	1.48	74.83	10.67	1.78	6.47	38.74	80.97	10.00	39.56

Table 22: Trojan filtering results (in %) of IF, VIF, AIF, and AIF without explicit trigger normalization (AIF\*) against noise-BI+ with different blending ratios ( $\alpha$ ) on CIFAR10. For a particular blending ratio and metric, the best result is highlighted in bold. Results taken from Tables 2, 14 are shown in italic.

poorer Ts on synthesized Trojan images (Fig. 22d) than AIF-w. On ground-truth Trojan images, AIF-w performs as well as AIF-w in terms of T (Fig. 22b) and worse than AIF-w in terms of  $\downarrow C$  (Fig. 22a) and  $\downarrow R$  (Fig. 22d).

### A.12. Explicit Normalization of Triggers in AIF

During training AIF, we observed that under the influence of  $\mathcal{L}_{VIF\text{-gen}}$  (Eq. 7), the norm  $\|m\|$  of a synthesized trigger mask  $m$  usually increases overtime despite the fact that  $\mathcal{L}_{VIF\text{-gen}}$  also contains a norm regularization term. The reason is that G is encouraged to output bigger Trojan triggers to fool F. However, too big trigger causes the generated Trojan image  $\tilde{x}$  to be very different from the input image  $x$ , which affects the learning of F. One way to deal with this problem is *explicitly normalizing*  $m$  so that its norm is always upper-bounded by  $\delta$ . Denoted by  $\bar{m}$  the  $\delta$ -normalized

version of  $m$ .  $\bar{m}$  can be computed as follows:

$$\bar{m} = \begin{cases} m & \text{if } \|m\| \leq \delta \\ \delta \frac{m}{\|m\|} & \text{if } \|m\| > \delta \end{cases} \quad (10)$$

or more compactly,

$$\begin{aligned} \bar{m} &= m \times \left( 1 - \frac{\max(\|m\| - \delta, 0)}{\|m\|} \right) \\ &= m \times \left( 1 - \frac{\text{ReLU}(\|m\| - \delta)}{\|m\|} \right) \end{aligned} \quad (11)$$

In case the norm is L2, the second expression in Eq. 10 can be seen as the projection of  $m$  onto the surface of a sphere of radius  $\delta$ . By replacing  $\text{ReLU}(\cdot)$  in Eq. 11 with  $\text{Softplus}(\cdot)$ ,

Dataset	Norm.	BadNet+			noise-BI+			image-BI+			InpAwAtk			WaNet		
		↓C	T	↓R	↓C	T	↓R	↓C	T	↓R	↓C	T	↓R	↓C	T	↓R
CIFAR10	w/	<b>5.60</b>	2.37	<b>9.03</b>	<b>4.87</b>	<i>1.14</i>	<b>6.02</b>	<b>5.23</b>	1.96	<b>7.10</b>	<b>5.28</b>	5.30	<i>11.87</i>	<b>4.30</b>	<b>1.22</b>	<b>5.67</b>
	wo/	5.90	<b>2.15</b>	10.00	5.60	<b>0.78</b>	7.50	6.60	<b>1.56</b>	7.53	6.20	<b>2.56</b>	<b>9.37</b>	5.80	2.22	8.10
GTSRB	w/	<b>-0.16</b>	<b>0.00</b>	<b>1.87</b>	<b>0.05</b>	<b>0.00</b>	<b>0.81</b>	<b>0.13</b>	7.47	9.54	<b>-0.03</b>	0.05	<b>1.37</b>	<b>-0.05</b>	0.50	<b>0.42</b>
	wo/	0.13	0.08	3.18	0.24	0.00	1.26	0.45	<b>0.92</b>	<b>5.44</b>	0.45	<b>0.00</b>	2.60	0.21	<b>0.11</b>	0.45

Table 23: Trojan filtering results (in %) of AIF with and without explicit trigger normalization against different attacks on CIFAR10 and GTSRB. For a particular attack, dataset and metric, the best result is highlighted in bold. Results taken from Table 2 are shown in italic.

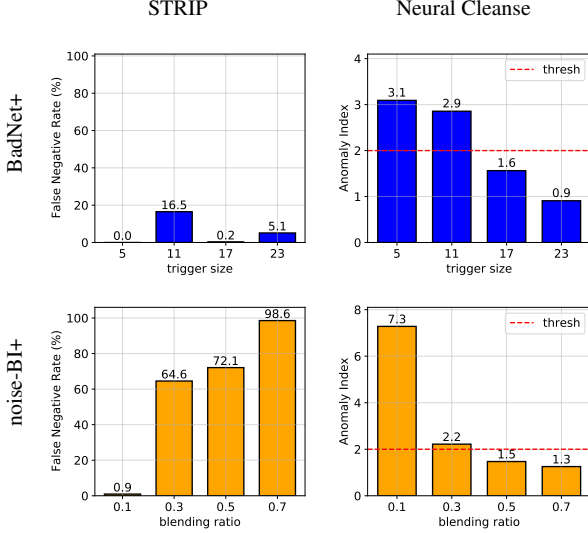


Figure 21: FNRs at 10% FPR of STRIP (left) and anomaly indices of Neural Cleanse (right) against BadNet+ with different trigger sizes (top) and noise-BI+ with different blending ratios (bottom).

we obtain a soft version of  $\bar{m}$ :

$$\begin{aligned} \bar{m}_s &= m \times \left( 1 - \frac{\text{Softplus}(\|m\| - \delta, \tau)}{\|m\|} \right) \\ &= m \times \left( 1 - \frac{\tau \log(1 + \exp((\|m\| - \delta)/\tau))}{\|m\|} \right) \end{aligned} \quad (12)$$

where  $\tau > 0$  is a temperature.  $\bar{m}_s$  with smaller  $\tau$  approximates  $\bar{m}$  better. Generally, using  $\bar{m}_s$  gives better gradient update than using  $\bar{m}$ . However, since Softplus is an upper-bound of ReLU,  $\text{Softplus}(\|m\| - \delta, \tau)$  can be greater than  $\|m\|$ , which causes  $\bar{m}_s$  to be negative. To avoid that, we slightly modify Eq. 12 into the equation below:

$$\bar{m}_s = m \times \left( 1 - \frac{\tau \log(1 + \exp((\|m\| - \delta)/\tau))}{\|m\| + \Omega} \right) \quad (13)$$

where  $\Omega > 0$  is an added term to ensure that  $\bar{m}_s \geq 0$ .  $\Omega$  can be computed from  $\tau$  and  $\delta$  by solving the following

inequality:

$$\begin{aligned} \tau \log(1 + \exp((\|m\| - \delta)/\tau)) &\leq \|m\| + \Omega \\ \Leftrightarrow 1 + \exp\left(\frac{\|m\| - \delta}{\tau}\right) &\leq \exp\left(\frac{\|m\| + \Omega}{\tau}\right) \\ \Leftrightarrow 1 &\leq \exp\left(\frac{\|m\|}{\tau}\right) \left( \exp\frac{\Omega}{\tau} - \exp\left(\frac{-\delta}{\tau}\right) \right) \\ \Leftrightarrow \exp\left(\frac{-\|m\|}{\tau}\right) &\leq \exp\frac{\Omega}{\tau} - \exp\left(\frac{-\delta}{\tau}\right) \end{aligned}$$

Since  $\exp\left(\frac{-\|m\|}{\tau}\right)$  is always smaller than 1, we can choose  $\Omega$  so that:

$$\begin{aligned} \exp\frac{\Omega}{\tau} - \exp\left(\frac{-\delta}{\tau}\right) &= 1 \\ \Leftrightarrow \Omega &= \tau \log\left(1 + \exp\left(\frac{-\delta}{\tau}\right)\right) \end{aligned}$$

In our experiments, we set  $\delta = 0.05$  and  $\tau = 0.01$ . We also observed that the hard normalization (Eq. 11) and the soft normalization (Eq. 13) of  $m$  give roughly the same performance.

### A.13. Visualization of Synthesized Trojan Images and Triggers

In Figs. 23a, 23b, and 23c, we visualize Trojan images (left) and triggers (right) synthesized by the three approaches in Section 3 with different generator’s architectures shown in Table 7 and different values of  $\lambda_0$  (Eq. 2). We observe that complex generators (D) usually produce finer triggers than simple generators (A) due to the better reconstruction capability. In addition, increasing  $\lambda$  results in triggers with smaller norms. However, none of these changes help us synthesize the true triggers.

### A.14. Qualitative Results of Our Filtering Defenses

#### A.14.1 Against Attacks with Normal Settings

In Figs. 24a, 25a, 26a, 27a, we show some ground-truth (GT) Trojan images  $\tilde{x}$  and their filtered counterparts  $\tilde{x}^\circ$  computed



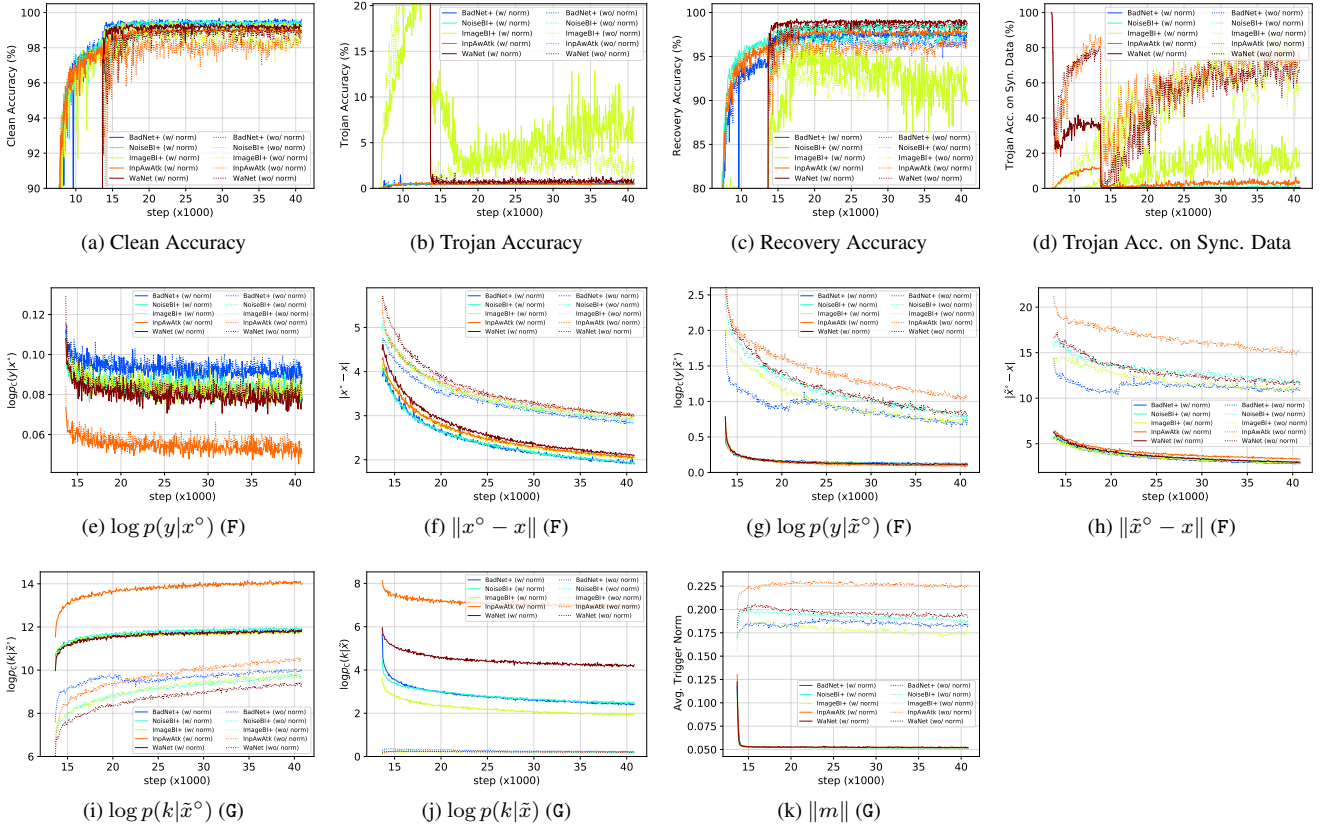


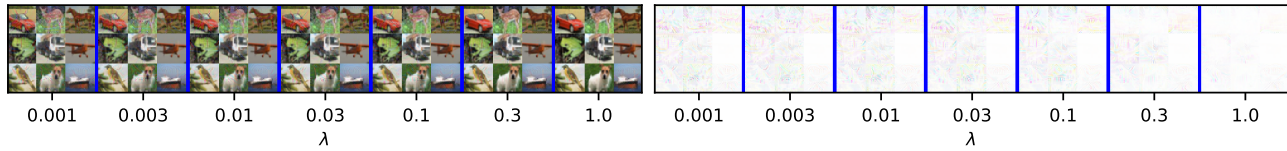
Figure 22: Test result curves and training loss curves of F, G of VIF with and without explicit trigger normalization against different attacks on GTSRB. These plots correspond to the results in the bottom 2 rows in Table 23.

by Februs (Feb.) and our filtering defenses (VIF, AIF) for different Trojan attacks and datasets. We also show the corresponding “counter-triggers” of  $\tilde{x}^\circ$  defined as  $|\tilde{x}^\circ - \tilde{x}|$  in Figs. 24b, 25b, 26b, 27b in comparison with the ground-truth Trojan triggers  $|\tilde{x} - x|$ . It is apparent that VIF and AIF correctly filter the true triggers of all the attacks without knowing them while Februs fails to filter the true triggers of noise-BI+, image-BI+, InpAwAtk and WaNet. The failure of Februs comes from the fact that GradCAM is unable to find regions containing full-sized, distributed triggers of InpAwAtk/WaNet. For BadNet+ and InpAwAtk, our filtering defenses mainly blur the triggers of these attacks instead of completely removing the triggers. This is enough to deactivate the triggers.

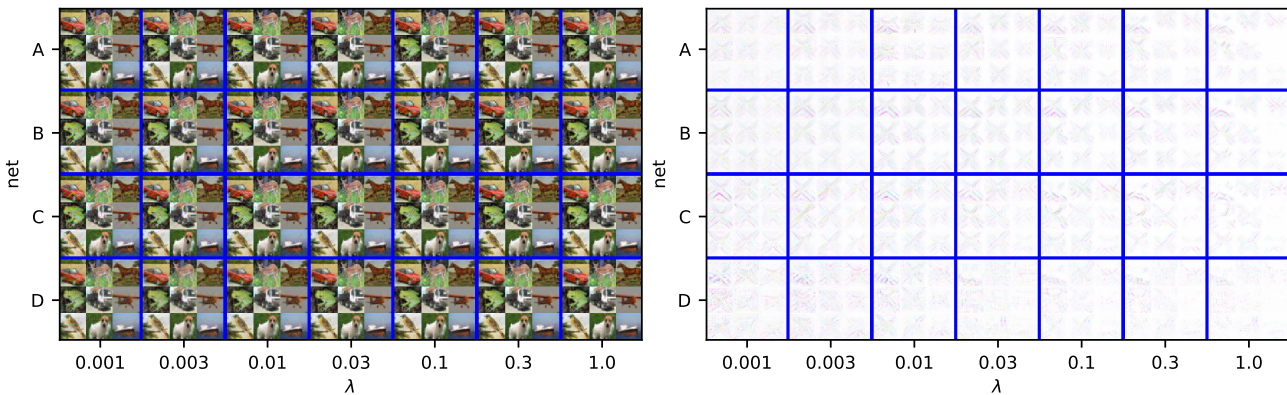
#### A.14.2 Against Attacks with Large-Norm Triggers

In Fig. 28, we visualize the filtered images and their corresponding counter-triggers computed by our methods for Trojan images of BadNet+ with different trigger sizes and of noise-BI+ with different blending ratios. In general, our

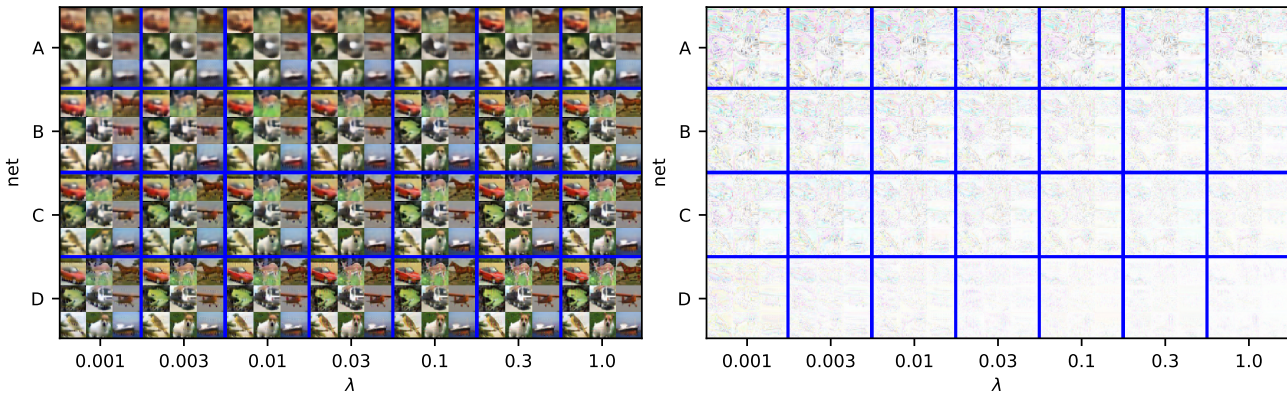
filtering defenses can effectively deactivate triggers embedded in the Trojan images via modifying the trigger pixels but cannot fully reconstruct the original clean images. These qualitative results correspond to the quantitative results in Tables 21, 22.



(a) Triggers as learnable parameters

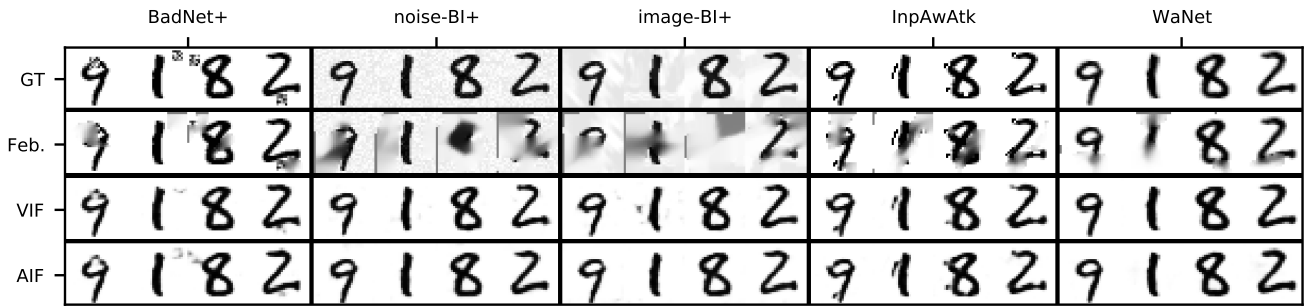


(b) Triggers synthesized via a trigger generator

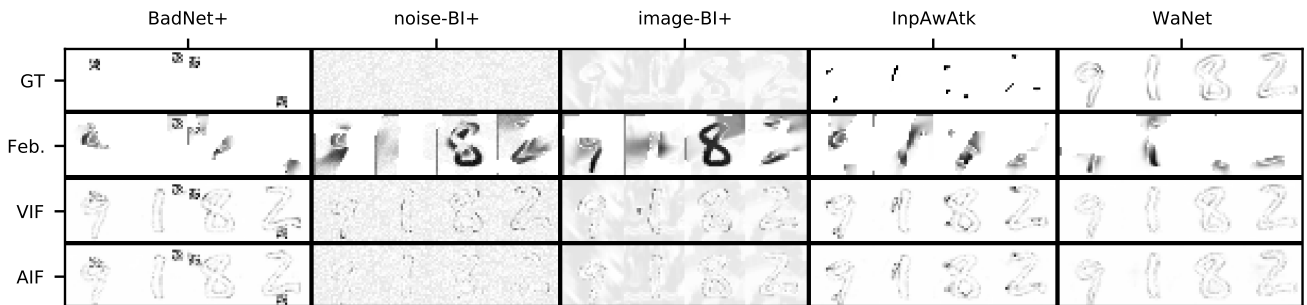


(c) Triggers computed via a Trojan-image autoencoder

Figure 23: Trojan images and triggers synthesized by the three approaches in Section 3. The dataset is CIFAR10. Trigger pixels are inverted for better visualization.



(a) Filtered images

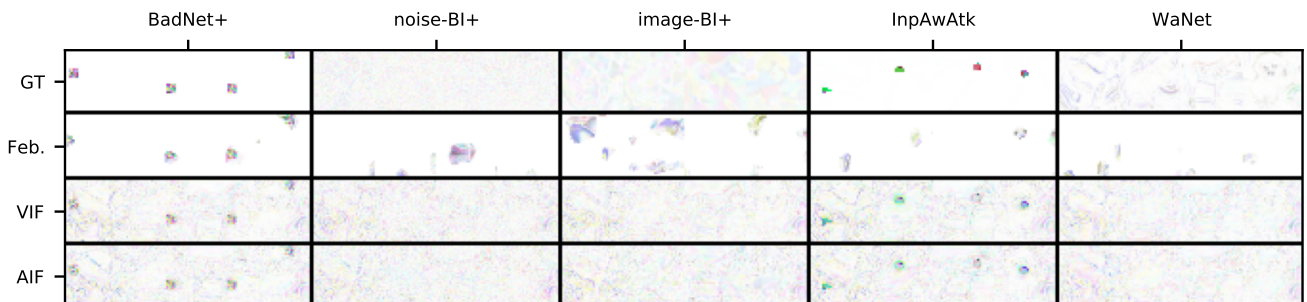


(b) Counter-triggers

Figure 24: (a): Ground-truth (GT) Trojan images of different attacks and the corresponding filtered images computed by Februus (Feb.), VIF, and AIF on MNIST. (b): GT triggers and counter-triggers w.r.t. the filtered images in (a).

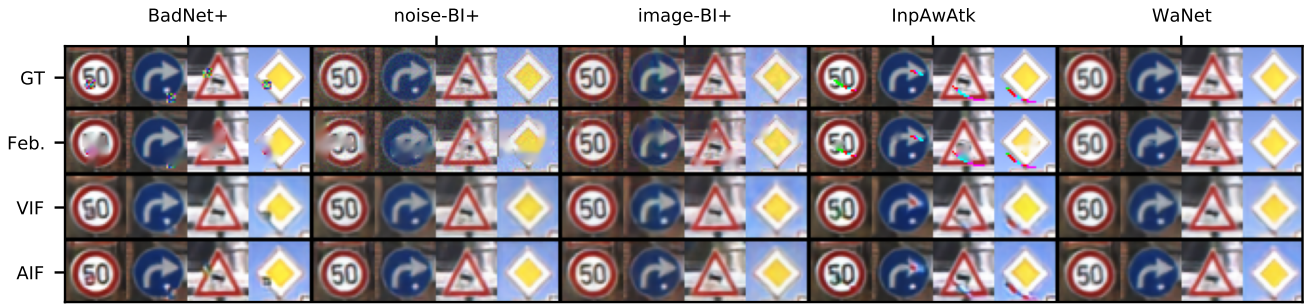


(a) Filtered images

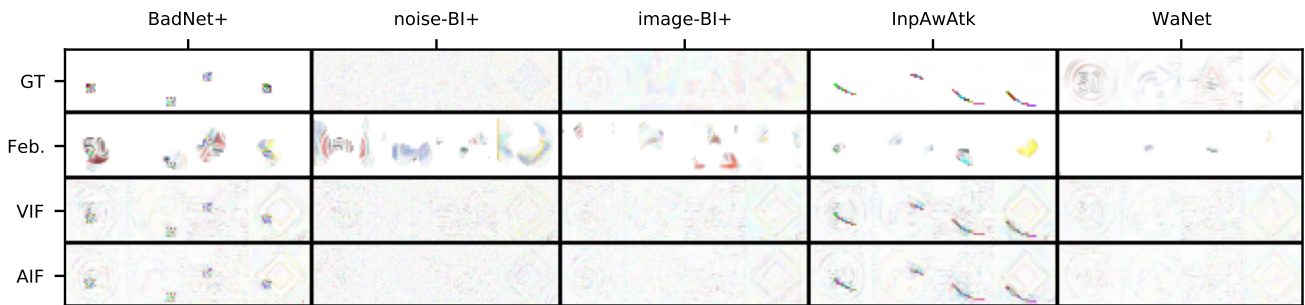


(b) Counter-triggers

Figure 25: (a): Ground-truth (GT) Trojan images of different attacks and the corresponding filtered images computed by Februus (Feb.), VIF, and AIF on CIFAR10. (b): GT triggers and counter-triggers w.r.t. the filtered images in (a).

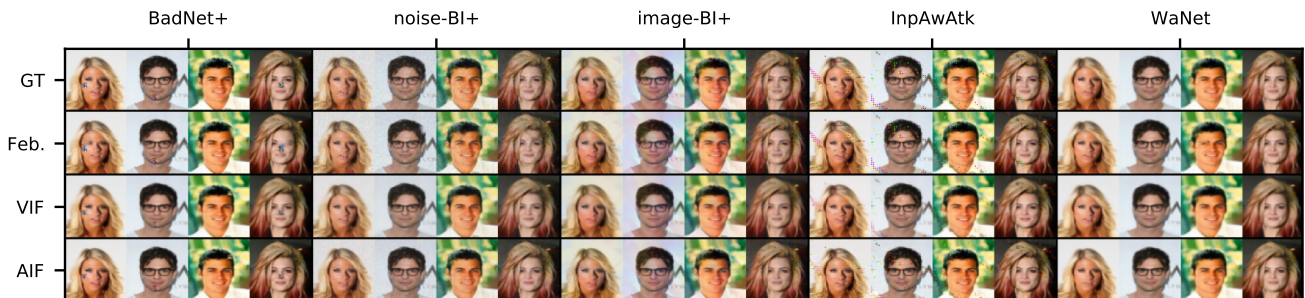


(a) Filtered images

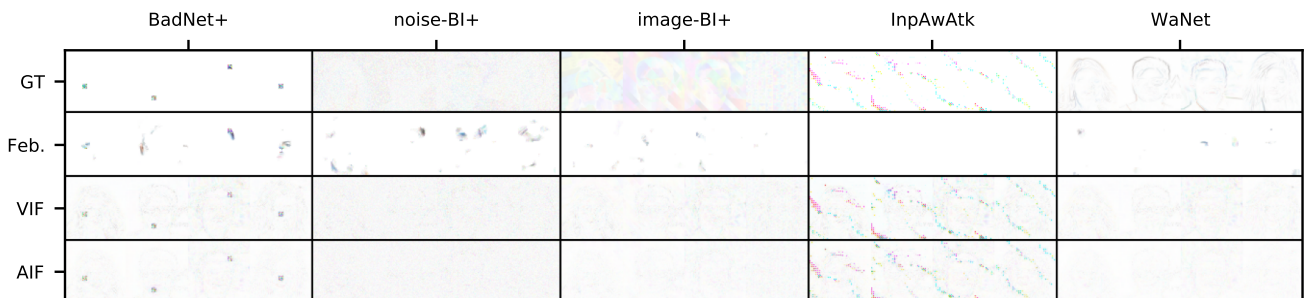


(b) Counter-triggers

Figure 26: (a): Ground-truth (GT) Trojan images of different attacks and the corresponding filtered images computed by Februs (Feb.), VIF, and AIF on GTSRB. (b): GT triggers and counter-triggers w.r.t. the filtered images in (a).



(a) Filtered images



(b) Counter-triggers

Figure 27: (a): Ground-truth (GT) Trojan images of different attacks and the corresponding filtered images computed by Februs (Feb.), VIF, and AIF on CelebA. (b): GT triggers and counter-triggers w.r.t. the filtered images in (a).

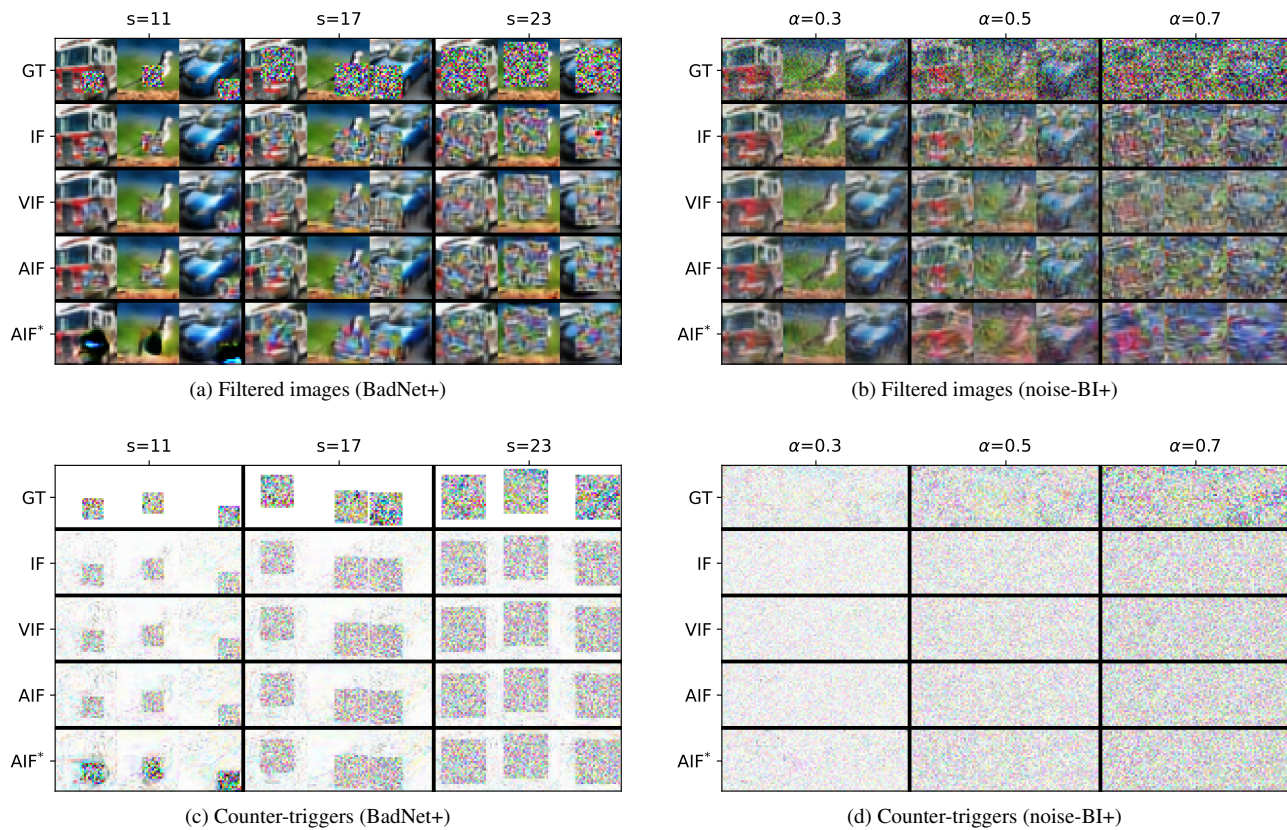


Figure 28: (a)/(b): Ground-truth (GT) Trojan images of BadNet+/noise-BI+ and the corresponding filtered images computed by IF, VIF, AIF, and AIF without explicit trigger normalization (AIF\*). (c)/(d): GT triggers and counter-triggers w.r.t. the filtered images in (a)/(b).